Efficient adaptive sampling applied to multivariate, multiple output rational interpolation models, with applications in electromagnetics-based device modelling

Robert Lehmensiek

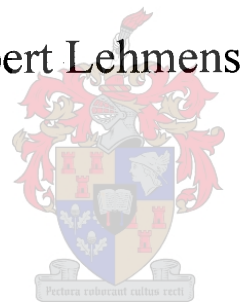

Dissertation presented for the degree of Doctor of Philosophy
in Engineering at the University of Stellenbosch

Promoter: Prof. P. Meyer *Date:* June 2001

DECLARATION

I, the undersigned, hereby declare that the work contained in this dissertation is my own original work and that I have not previously in its entirety or in part submitted it at any university for a degree.

Signature: R. Lehmensiek Date: 7/6/2001

ABSTRACT

Keywords: Multivariate rational interpolation, multivariate adaptive sampling, model-based parameter estimation, surrogate modelling, computer-aided design.

A robust and efficient adaptive sampling algorithm for multivariate, multiple output rational interpolation models, based on convergents of Thiele-type branched continued fractions, is presented. A variation of the standard branched continued fraction method is proposed that uses approximation to establish a non-rectangular grid of support points. Starting with a low order interpolant, the technique systematically increases the order by optimally choosing new support points in the areas of highest error, until the desired accuracy is achieved. In this way, accurate surrogate models are established by a small number of support points, without assuming any *a priori* knowledge of the microwave structure under study. The technique is illustrated and evaluated on several passive microwave structures, however it is general enough to be applied to many modelling problems.

OPSOMMING

Sleutelwoorde: Multi-veranderlike rasionale interpolasie, multi-veranderlike aanpasbare monsterneming, model-gebaseerde parameter afskatting, surrogaat modelering, rekenaargesteunde ontwerp.

'n Robuuste en effektiewe aanpasbare monsternemingsalgoritme vir multi-veranderlike, multi-uittree rasionale interpolasiemodelle, gegrond op konvergente van Thiele vertakte volgehoue breukuitbreidings, word beskryf. 'n Variasie op die konvensionele breukuitbreidingsmetode word voorgestel, wat 'n nie-reghoekige rooster van ondersteuningspunte gebruik in die funksiebenadering. Met 'n lae orde interpolant as beginpunt, verhoog die algoritme stelselmatig die orde van die interpolant deur optimal verbeterde ondersteuningspunte te kies waar die grootste fout voorkom, totdat die gewensde akuraatheid bereik word. Hierdeur word akkurate surrogaat modelle opgebou ten spyte van min inisiële ondersteuningspunte, asook sonder voorkennis van die mikrogolfstruktuur ter sprake. Die algoritme word gedemonstreer en geëvalueer op verskeie passiewe mikrogolfstrukture, maar is veelsydig genoeg om toepassing te vind in meer algemene modelleringsprobleme.

ACKNOWLEDGEMENTS

I want to express my sincere gratitude to everyone who has contributed to this dissertation in any way and in particular, I want to thank:

- my promoter, Prof. Petrie Meyer, for his help, advice and guidance;
- Prof. Dr. Annie Cuyt, University of Antwerp, Belgium, for insightful discussions on multivariate rational interpolants;
- Reutech Radar Systems, for allowing me the opportunity to do this study;
- Graham, for proofreading the thesis;
- L. J., for helping with the Afrikaans translation;
- Karin, for her patience and loving support.

CONTENTS

CHAPTER 1: INTRODUCTION

1.1 Introduction

The increasing need of a first-pass success level to reduce the cost of the design of microwave circuits has placed enhanced demands on computer-aided design (CAD) tools. Furthermore, the stringent design specifications and the inclusion of effects such as manufacturing tolerances in the design necessitates the use of optimisation-based computer algorithms and statistical analysis methods such as Monte Carlo analysis and yield-driven optimisation. This leads to a highly repetitive computational process, i.e. numerous evaluations of a model of the physical structure being designed. Hence, a model of the microwave structure is required that is not only highly accurate, but also computationally effective.

Computational electromagnetic (CEM) analysis techniques, which are computer solutions of Maxwell's equations, can provide models with high accuracy for a microwave structure over a certain range of frequency and/or physical dimensions. However, the computational effort required can become excessive, especially for large and complex structures. Empirical circuit-theoretic models, if they exist, are computationally very effective, but their accuracy over a wide band and particularly at higher frequencies becomes questionable due to their inability to model all parasitic and coupling effects. New modelling techniques that establish surrogate models for microwave structures provide a solution to this predicament. Since surrogate models directly fit data from CEM simulations, their model accuracy is high, and the evaluation of surrogate models is fast, allowing highly repetitive model evaluations in optimisation and yield-driven design. Current models include look-up tables, interpolation techniques and artificial neural networks [1], [2].

Look-up tables require the generation of a database, where data points are determined in a multi-dimensional (usually uniform) grid, and the amount of storage space increases exponentially as the dimension increases. The number and selection of these data points may not be optimal, which leads to inaccurate modelling or oversampling. Usually low order polynomial interpolation techniques are employed to determine values between grid points and hence only mild non-linearities can be handled [3], [4].

Artificial neural networks are massively connected parallel networks of simple processing units called neurons, with an input/output mapping being represented in the form of interconnection weights. Their design mimics the organisation and performance of biological neural networks in the nervous system of the brain. Artificial neural networks can learn and generalise from data, are

easy to implement and are very fast to evaluate. Once properly selected and trained, they have the ability to model highly non-linear functions with high dimensionality, since the size of the neural network does not increase exponentially with dimension. However, they require networks with the right topology, high numbers of training and testing examples, and often excessive training times [5], [6].

Interpolation techniques, as artificial neural networks, require only storage of the interpolant coefficients, and in addition normally require the smallest amount of data, i.e. CEM analyses, to establish a model. Therefore, model building can be much faster than look-up table or neural network models. Interpolation models are fast to evaluate and hence are well suited for circuit optimisation and statistical design [7]-[10].

1.2 Interpolation models

While polynomial functions are often used as interpolants, rational functions yield better results for functions containing poles or for meromorphic functions. Polynomial interpolation is prone to wild oscillations and an acceptable accuracy is sometimes achieved only by polynomials of intolerably high degree [11], [12].

A rational function can be constructed by calculating the explicit solution of a system of interpolatory conditions, by starting a recursive algorithm, or by calculating the convergent of a continued fraction [13], [14]. The use of continued fractions as interpolants is a computationally efficient method [15] and gives accurate numerical results [16], [17]. Recursive algorithms on the other hand, are accurate, but determine a value of the interpolant directly from tabulated data without calculating the coefficients. Hence, they become computationally inefficient for a large number of function evaluations. This method was applied in [18] using the Bulirsch-Stoer algorithm [19]. The technique of solving a system of interpolatory conditions, while used most often [18], [20]-[28], is generally accepted to be the least accurate method. Usually a least squares fit is used. In [21] and [29] the authors used the total least squares method, which allows for some suppression of the effects of noise in the data. Several authors have applied the interpolation technique to the method of moments, for which derivatives with respect to frequency can be calculated and integrated into the interpolation model [20]-[22].

The orders of interpolants are generally determined heuristically or estimated. With no *a priori* knowledge of the problem, this can easily lead to over-determined interpolants, requiring high numbers of support points. When CEM techniques are used for the generation of the support

points, it is of utmost importance to minimise the required number, especially for the multi-variable case. This can only be achieved by the use of adaptive sampling schemes, where the order of the function is gradually increased until a desired accuracy is reached. In turn, this requires that a suitable error function exists and that unequally spaced support points can be used [30]. Published error functions include the difference between two interpolation models that either use different data sample sets and/or are of different rational polynomial orders [18], [23], [25], [26].

The extension of a single variable rational interpolant to a multi-variable rational interpolant is not trivial since a large degree of freedom in the choice for the numerator and denominator polynomials exists. Only a few multivariate sampling algorithms have been published. In [18] the authors use a rectangular grid of support points and recursive univariate interpolation to establish the multidimensional interpolation space. They also mention establishing a multivariate function by solving a linear system of equations. In [26] multivariate polynomials are used to build a model for the geometrical parameters at a single frequency and rational interpolation is used to combine these polynomials to determine the entire interpolation space.

In this dissertation a novel adaptive sampling algorithm for general multivariate interpolation models is presented. The interpolation model is based on a Thiele-type branched continued fraction representation of a multivariate rational function. The coefficients of the rational interpolant and the evaluation of the function values are determined in a recursive manner, providing a computationally efficient and numerically accurate interpolation technique. The standard branched continued fraction interpolation technique, which requires a fully filled rectangular grid of support points, is adapted here to allow sampling on a non-rectangular grid. Support points can therefore be placed optimally in the interpolation space, which will result in a reduction of the number of CEM analyses. An error estimate is obtained as a natural consequence of the recursion formulas. The proposed technique constructs sets of single parameter interpolants at optimal points in a (D−1)-variable space. The univariate interpolants are in turn used to form bivariate, trivariate and finally D-variable functions. Starting with low order interpolants, the adaptive sampling algorithm systematically increases the order by optimally choosing new support points in the areas of highest error, until a mathematical model with the required accuracy is achieved.

To model multi-port microwave discontinuities, a multiple output interpolation model is defined, which consists of a set of rational interpolants, where each interpolant models one of the output parameters/ports. For this case, a single global error function is defined incorporating all the output parameters, and is used for the selection of the same set of support points for all the interpolants.

The algorithm is fully automatic, does not require derivatives and is widely applicable. The technique is evaluated on several passive microwave structures with errors of less than 0.25 % being achieved in all cases. This model accuracy is more than adequate for the purposes of designing most microwave circuits.

1.3 About the dissertation

The aim of this dissertation is to develop the theory for an adaptive sampling algorithm for multivariate, multiple output rational interpolation models and to investigate the numerical performance. Use is made of several CEM analysis techniques, which are referenced, but are not discussed as the mathematical derivations of these techniques are beyond the scope of this dissertation.

The primary original contributions of this work are [31]-[35]:

- the development of a robust adaptive sampling algorithm for interpolation models,
- the extension to multivariate interpolation models,
- the extension to multiple output interpolation models.

The secondary contributions are:

- the adaptation of the standard branched continued fraction to allow a non-rectangular grid of support points,
- the application of accurate and computationally efficient multivariate rational interpolants, represented by Thiele-type branched continued fractions, to the modelling of electromagnetics-based devices,
- the application of the method to aggressive space mapping [31],
- the application of the method to root-finding [32].

The theory of Thiele-type branched continued fractions has been presented for the bivariate case in [36] and it is generalised for the multivariate case in chapter 2 of this dissertation. The multivariate adaptive sampling algorithm for the interpolant presented in chapter 2 is expounded in chapter 3. The proposed technique is evaluated in chapter 4 for the univariate case and in chapter 5 for the multivariate case by applying it to several electromagnetics-based device modelling problems. Finally, chapter 6 contains possible extensions to the theory presented here and a conclusion.

CHAPTER 2: RATIONAL INTERPOLATION

The multivariate interpolation used in this dissertation, has as starting point the more simple univariate rational interpolation. In order to ease understanding of the former, a detailed exposition of the latter is first given.

2.1 Univariate Rational Interpolation

Rational interpolation defines an analytic function $\Re$ of the complex variable γ as a quotient of two polynomials $N_\zeta(\gamma)$ and $D_\upsilon(\gamma)$,

$$\Re(\gamma) = \frac{N_\zeta(\gamma)}{D_\upsilon(\gamma)} = \frac{\sum_{k=0}^{\zeta} p_k \gamma^k}{\sum_{k=0}^{\upsilon} q_k \gamma^k}, \tag{1}$$

with ζ the order of the numerator, υ the order of the denominator, and p_k and q_k the polynomial coefficients. The rational interpolant $\Re$ provides an approximation on an interval $[\gamma^{(0)}, \gamma^{(1)}]$ of the function $S(\gamma)$ that we are trying to model. Since there are $\zeta+\upsilon+1$ unknown coefficients (q_0 is chosen arbitrarily), a set of $N+1=\zeta+\upsilon+1$ support points $(\gamma^{(i)}; S_i)$, with $i=0, 1, \cdots, N$ and $S_i = S(\gamma^{(i)})$, are required to completely determine $\Re(\gamma)$. $\Re(\gamma)$ is then a curve passing through the ordinates S_i at the abscissas $\gamma^{(i)}$ for $i=0, 1, \cdots, N$. It is assumed that $\Re(\gamma)$ exists and has no unattainable support points [37], [38].

Equation (1) is represented by a convergent of a corresponding Thiele continued fraction, as shown in equation (2). Each rational expression $\Re_k(\gamma)$ is a k^{th} order partial fraction expansion of equation (1), together constituting a set of interpolants which exhibit increasing accuracy as k increases, reaching a convergent value at $k=N$.

$$\begin{aligned}\Re_k(\gamma) &= S_0 + \cfrac{\gamma-\gamma^{(0)}}{\varphi_1(\gamma^{(1)},\gamma^{(0)}) + \cfrac{\gamma-\gamma^{(1)}}{\varphi_2(\gamma^{(2)},\gamma^{(1)},\gamma^{(0)}) + \ldots \\ \qquad \ldots + \cfrac{\gamma-\gamma^{(k-1)}}{\varphi_k(\gamma^{(k)},\gamma^{(k-1)},\cdots,\gamma^{(0)})}}} \\ &= S_0 + \sum_{i=1}^{k} \left| \frac{\gamma-\gamma^{(i-1)}}{\varphi_i(\gamma^{(i)},\gamma^{(i-1)},\cdots,\gamma^{(0)})} \right|, \qquad k=0, 1, \cdots, N \end{aligned} \tag{2}$$

The inverse differences φ_k, are the partial denominators of equation (2), and are essentially the coefficients that define $\Re_k(\gamma)$. The inverse differences are determined recursively from the support

points and are defined in equation (3) [19].

$$\varphi_1(\gamma^{(i)},\gamma^{(0)}) \equiv \frac{\gamma^{(i)}-\gamma^{(0)}}{S_i - S_0}, \qquad i=1,2,\cdots,N$$

$$\varphi_k(\gamma^{(i)},\gamma^{(k-1)},\cdots,\gamma^{(0)}) \equiv \frac{\gamma^{(i)}-\gamma^{(k-1)}}{\varphi_{k-1}(\gamma^{(i)},\gamma^{(k-2)},\cdots,\gamma^{(0)}) - \varphi_{k-1}(\gamma^{(k-1)},\gamma^{(k-2)},\cdots,\gamma^{(0)})}, \qquad i=k,k+1,\cdots,N;\ k=2,3,\cdots,N \tag{3}$$

The interpolation function $\Re_k(\gamma)$ can be evaluated numerically with the three-term recurrence relations given in equation (4) initialised with $N_0(\gamma)=S_0$, $N_1(\gamma)=\varphi_1(\gamma^{(1)},\gamma^{(0)})N_0+(\gamma-\gamma^{(0)})$, $D_0(\gamma)=1$, and $D_1(\gamma)=\varphi_1(\gamma^{(1)},\gamma^{(0)})$ [39]. As a consequence of the continued fraction formulation $\zeta=\upsilon=k/2$ for k even and $\zeta=(k+1)/2$ and $\upsilon=(k-1)/2$ for k odd.

$$\left.\begin{aligned} N_k(\gamma) &= \varphi_k(\gamma^{(k)},\gamma^{(k-1)},\cdots,\gamma^{(0)})N_{k-1}(\gamma)+(\gamma-\gamma^{(k-1)})N_{k-2}(\gamma) \\ D_k(\gamma) &= \varphi_k(\gamma^{(k)},\gamma^{(k-1)},\cdots,\gamma^{(0)})D_{k-1}(\gamma)+(\gamma-\gamma^{(k-1)})D_{k-2}(\gamma) \end{aligned}\right\} \quad k=2,3,\cdots,N$$

$$\Re_k(\gamma) = \frac{N_k(\gamma)}{D_k(\gamma)} \qquad k=0,1,\cdots,N \tag{4}$$

The derivative of $\Re_k(\gamma)$ with respect to γ can be calculated recursively by taking the derivatives of equation (4), initialised with $\frac{\partial N_0(\gamma)}{\partial\gamma}=0$, $\frac{\partial D_0(\gamma)}{\partial\gamma}=0$, $\frac{\partial N_1(\gamma)}{\partial\gamma}=1$ and $\frac{\partial D_1(\gamma)}{\partial\gamma}=0$, i.e.

$$\left.\begin{aligned} \frac{\partial N_k(\gamma)}{\partial\gamma} &= \varphi_k(\gamma_k,\gamma_{k-1},\cdots,\gamma_0)\frac{\partial N_{k-1}(\gamma)}{\partial\gamma}+(\gamma-\gamma_{k-1})\frac{\partial N_{k-2}(\gamma)}{\partial\gamma}+N_{k-2}(\gamma) \\ \frac{\partial D_k(\gamma)}{\partial\gamma} &= \varphi_k(\gamma_k,\gamma_{k-1},\cdots,\gamma_0)\frac{\partial D_{k-1}(\gamma)}{\partial\gamma}+(\gamma-\gamma_{k-1})\frac{\partial D_{k-2}(\gamma)}{\partial\gamma}+D_{k-2}(\gamma) \end{aligned}\right\} \quad k=2,3,\cdots,N$$

$$\frac{\partial\Re_k(\gamma)}{\partial\gamma} = \frac{D_k(\gamma)\frac{\partial N_k(\gamma)}{\partial\gamma} - N_k(\gamma)\frac{\partial D_k(\gamma)}{\partial\gamma}}{D_k^{\,2}(\gamma)} \qquad k=1,2,\cdots,N. \tag{5}$$

Similarly, all higher order derivatives of $\Re_k(\gamma)$ can be calculated.

The computational effort in determining the coefficients $\varphi_k(\gamma_k,\gamma_{k-1},\cdots,\gamma_0)$ for $k=1,2,\cdots,N$ using the recurrence relations in equation (3), is ½N(N+1) divisions and N(N+1) subtractions. To evaluate $N_N(\gamma)$ or $D_N(\gamma)$ with the recurrence relations in equation (4), requires 2N–1 multiplications, N additions and N subtractions. In total, to evaluate $\Re_N(\gamma)$ requires 4N–2 multiplications, 1 division, 2N additions and 2N subtractions.

As the accuracy of $\Re(\gamma)$ over a certain γ range is required to increase, the order of the interpolating rational polynomial increases. This increase in the degree of freedom of $\Re(\gamma)$ can cause a zero in the numerator and a zero in the denominator polynomials to occur at almost precisely the same position. At these pole/zero combinations L'Hospital's rule is applied for the evaluation of the interpolation function, i.e. $\Re_k(\gamma)\rightarrow\frac{\partial N_k(\gamma)}{\partial\gamma}\Big/\frac{\partial D_k(\gamma)}{\partial\gamma}$.

2.2 Multivariate Rational Interpolation

The multivariate rational function is defined in equation (6), where γ_d, with $d=1,2,\cdots,D$, represents the D complex variables. The interpolation function $\Re(\gamma_1,\gamma_2,\cdots,\gamma_D)$ will be equal at the support points to the function $S(\gamma_1,\gamma_2,\cdots,\gamma_D)$, that is being modelled, and will approximate $S(\gamma_1,\gamma_2,\cdots,\gamma_D)$ between the support points. The set of support points are represented by $(\gamma_1^{(i_1)},\gamma_2^{(i_2)},\cdots,\gamma_D^{(i_D)};S_{i_1,i_2,\cdots,i_D})$; $i_d=0,1,\cdots,N_d$, $d=1,2,\cdots,D$, and $S_{i_1,i_2,\cdots,i_D}=S(\gamma_1^{(i_1)},\gamma_2^{(i_2)},\cdots,\gamma_D^{(i_D)})$. For the moment it is assumed that the support points are placed on a fully filled, not necessarily equidistant, rectangular grid, and hence the full set is given by the Cartesian product of the support points for each variable, i.e. $\{\gamma_1^{(0)},\gamma_1^{(1)},\cdots,\gamma_1^{(N_1)}\}\times\{\gamma_2^{(0)},\gamma_2^{(1)},\cdots,\gamma_2^{(N_2)}\}\times\cdots\times\{\gamma_D^{(0)},\gamma_D^{(1)},\cdots,\gamma_D^{(N_D)}\}$. A method analogous to the univariate case for determination and evaluation of the multivariate rational interpolant is used. In the following paragraphs the generic equations for the multivariate rational interpolation technique are given. In the literature these equations are given exclusively for the bivariate case.

$$\Re(\gamma_1,\gamma_2,\cdots,\gamma_D)=\frac{N(\gamma_1,\gamma_2,\cdots,\gamma_D)}{D(\gamma_1,\gamma_2,\cdots,\gamma_D)} \tag{6}$$

The interpolation function $\Re(\gamma_1,\gamma_2,\cdots,\gamma_D)$ is represented by the convergent of a multivariate Thiele-type branched continued fraction of the form

$$\Re(\gamma_1,\gamma_2,\cdots,\gamma_D)=\Re_0(\gamma_2,\gamma_3,\cdots,\gamma_D\,|\,\gamma_1^{(0)})+\sum_{i_1=1}^{N_1}\frac{\gamma_1-\gamma_1^{(i_1-1)}}{\Re_{i_1}(\gamma_2,\gamma_3,\cdots,\gamma_D\,|\,\gamma_1^{(i_1)})}. \tag{7}$$

Note the use of $f(\gamma_j|\gamma_i)$ to indicate a function f of variable γ_j with γ_i being defined for the function $f(\gamma_i,\gamma_j)$.

Compared to the univariate continued fraction, equation (2), each of the constant partial denominators is replaced with a multivariate function $\Re_{i_1}(\gamma_2,\gamma_3,\cdots,\gamma_D\,|\,\gamma_1^{(i_1)})$, which has one less variable than $\Re(\gamma_1,\gamma_2,\cdots,\gamma_D)$ and is defined with γ_1 constant and equal to $\gamma_1^{(i_1)}$. Each $\Re_{i_1}(\gamma_2,\gamma_3,\cdots,\gamma_D\,|\,\gamma_1^{(i_1)})$ can in turn be represented by a continued fraction as shown in equation (8), where $\Re_{i_2}(\gamma_3,\gamma_4,\cdots,\gamma_D\,|\,\gamma_1^{(i_1)},\gamma_2^{(i_2)})$ is defined at $\gamma_1=\gamma_1^{(i_1)}$ and $\gamma_2=\gamma_2^{(i_2)}$.

$$\Re_{i_1}(\gamma_2,\gamma_3,\cdots,\gamma_D\,|\,\gamma_1^{(i_1)})=\Re_0(\gamma_3,\gamma_4,\cdots,\gamma_D\,|\,\gamma_1^{(i_1)},\gamma_2^{(0)})+\sum_{i_2=1}^{N_2}\frac{\gamma_2-\gamma_2^{(i_2-1)}}{\Re_{i_2}(\gamma_3,\gamma_4,\cdots,\gamma_D\,|\,\gamma_1^{(i_1)},\gamma_2^{(i_2)})},$$

$$i_1=0,1,\cdots,N_1 \tag{8}$$

The substitution of the partial denominators by continued fractions is repeatedly performed

according to equation (9). The number of variables of $\Re_{i_d}(\gamma_{d+1}, \gamma_{d+2}, \cdots, \gamma_D \mid \gamma_1^{(i_1)}, \gamma_2^{(i_2)}, \cdots, \gamma_d^{(i_d)})$ decreases with every step until this function becomes a univariate function $\Re_{i_d}(\gamma_D \mid \gamma_1^{(i_1)}, \gamma_2^{(i_2)}, \cdots, \gamma_{D-1}^{(i_{D-1})})$, in which case equation (3) is used to determine its coefficients and equation (4) is used to evaluate it.

$$\Re_{i_{d-1}}(\gamma_d, \gamma_{d+1}, \cdots, \gamma_D \mid \gamma_1^{(i_1)}, \gamma_2^{(i_2)}, \cdots, \gamma_{d-1}^{(i_{d-1})}) =$$

$$\Re_0(\gamma_{d+1}, \gamma_{d+2}, \cdots, \gamma_D \mid \gamma_1^{(i_1)}, \gamma_2^{(i_2)}, \cdots, \gamma_d^{(0)}) + \sum_{i_d=1}^{N_d} \frac{\gamma_d - \gamma_d^{(i_d-1)}}{\left| \Re_{i_d}(\gamma_{d+1}, \gamma_{d+2}, \cdots, \gamma_D \mid \gamma_1^{(i_1)}, \gamma_2^{(i_2)}, \cdots, \gamma_d^{(i_d)}) \right|},$$

$$i_{d-1} = 0, 1, \cdots, N_{d-1}, \; d = 2, 3, \cdots, D-1 \quad (9)$$

The computation of the above multivariate continued fraction follows a tree-like structure, and is therefore called a branched continued fraction (BCF). Different forms of BCFs can be constructed, depending on the way in which the list of support points is enumerated [40]-[42]. The BCF used in this dissertation was defined by Siemaszko [36].

Similar to the univariate case, each of the BCFs of equations (7), (8) and (9) can be evaluated by using three-term recurrence relations given in equation (10) for $d = 1, 2, \cdots, D-1$, initialised with:

$$N_0(\gamma_d, \gamma_{d+1}, \cdots, \gamma_D) = \Re_0(\gamma_{d+1}, \gamma_{d+2}, \cdots, \gamma_D \mid \gamma_1^{(i_1)}, \gamma_2^{(i_2)}, \cdots, \gamma_d^{(0)}),$$

$$D_0(\gamma_d, \gamma_{d+1}, \cdots, \gamma_M) = 1,$$

$$N_1(\gamma_d, \gamma_{d+1}, \cdots, \gamma_D) = \Re_1(\gamma_{d+1}, \gamma_{d+2}, \cdots, \gamma_D \mid \gamma_1^{(i_1)}, \gamma_2^{(i_2)}, \cdots, \gamma_d^{(1)}) N_0(\gamma_d, \gamma_{d+1}, \cdots, \gamma_D) + (\gamma_d - \gamma_d^{(0)}) \text{ and}$$

$$D_1(\gamma_d, \gamma_{d+1}, \cdots, \gamma_D) = \Re_1(\gamma_{d+1}, \gamma_{d+2}, \cdots, \gamma_D \mid \gamma_1^{(i_1)}, \gamma_2^{(i_2)}, \cdots, \gamma_d^{(1)}).$$

$$\left.\begin{aligned} N_k(\gamma_d, \gamma_{d+1}, \cdots, \gamma_D) = \\ \Re_k(\gamma_{d+1}, \gamma_{d+2}, \cdots, \gamma_D \mid \gamma_1^{(i_1)}, \gamma_2^{(i_2)}, \cdots, \gamma_d^{(k)}) N_{k-1}(\gamma_d, \gamma_{d+1}, \cdots, \gamma_D) + (\gamma_d - \gamma_d^{(k-1)}) N_{k-2}(\gamma_d, \gamma_{d+1}, \cdots, \gamma_D) \\ D_k(\gamma_d, \gamma_{d+1}, \cdots, \gamma_D) = \\ \Re_k(\gamma_{d+1}, \gamma_{d+2}, \cdots, \gamma_D \mid \gamma_1^{(i_1)}, \gamma_2^{(i_2)}, \cdots, \gamma_d^{(k)}) D_{k-1}(\gamma_d, \gamma_{d+1}, \cdots, \gamma_D) + (\gamma_d - \gamma_d^{(k-1)}) D_{k-2}(\gamma_d, \gamma_{d+1}, \cdots, \gamma_D) \end{aligned}\right\} \quad (10)$$

$$k = 2, 3, \cdots, N_d$$

$$\Re_k(\gamma_d, \gamma_{d+1}, \cdots, \gamma_D \mid \gamma_1^{(i_1)}, \gamma_2^{(i_2)}, \cdots, \gamma_{d-1}^{(i_{d-1})}) = \frac{N_k(\gamma_d, \gamma_{d+1}, \cdots, \gamma_D)}{D_k(\gamma_d, \gamma_{d+1}, \cdots, \gamma_D)} \qquad k = 0, 1, \cdots, N_d$$

In this case sets of support points are combined to define sets of univariate interpolation functions with D–1 variables constant. The union of these univariate interpolation functions then generates sets of bivariate functions. Sets of bivariate functions combine to form three-variable interpolation functions. The process is repeated until a multivariate interpolation function with D variables is determined.

From the above formulation it follows that the determination of the coefficients for the multivariate interpolant is equivalent to the determination of coefficients for a set of univariate functions. These univariate functions are determined by repeatedly applying the set of recurrence relations given in equation (11) for $d=1,2,\cdots,\mathrm{D}-1$.

$$\xi_0(\gamma_d^{(i)};\gamma_{d+1},\gamma_{d+2},\cdots,\gamma_{\mathrm{D}}) \equiv \mathrm{S}(\gamma_1^{(i_1)},\gamma_2^{(i_2)},\cdots,\gamma_d^{(i)},\gamma_{d+1},\cdots,\gamma_{\mathrm{D}}),$$

$$\xi_1(\gamma_d^{(i)},\gamma_d^{(0)};\gamma_{d+1},\gamma_{d+2},\cdots,\gamma_{\mathrm{D}}) \equiv \frac{\gamma_d^{(i)}-\gamma_d^{(0)}}{\xi_0(\gamma_d^{(i)};\gamma_{d+1},\gamma_{d+2},\cdots,\gamma_{\mathrm{D}})-\xi_0(\gamma_d^{(0)};\gamma_{d+1},\gamma_{d+2},\cdots,\gamma_{\mathrm{D}})}, \qquad i=1,2,\cdots,\mathrm{N}_d \quad (11)$$

$$\xi_k(\gamma_d^{(i)},\gamma_d^{(k-1)},\cdots,\gamma_d^{(0)};\gamma_{d+1},\gamma_{d+2},\cdots,\gamma_{\mathrm{D}}) \equiv$$
$$\frac{\gamma_d^{(i)}-\gamma_d^{(k-1)}}{\xi_{k-1}(\gamma_d^{(i)},\gamma_d^{(k-2)},\cdots,\gamma_d^{(0)};\gamma_{d+1},\gamma_{d+2},\cdots,\gamma_{\mathrm{D}})-\xi_{k-1}(\gamma_d^{(k-1)},\gamma_d^{(k-2)},\cdots,\gamma_d^{(0)};\gamma_{d+1},\gamma_{d+2},\cdots,\gamma_{\mathrm{D}})},$$
$$i=k,k+1,\cdots,\mathrm{N}_d;\ k=2,3,\cdots,\mathrm{N}_d$$

Then,

$$\Re_{i_d}(\gamma_{d+1},\gamma_{d+2},\cdots,\gamma_{\mathrm{D}}\,|\,\gamma_1^{(i_1)},\gamma_2^{(i_2)},\cdots,\gamma_d^{(i_d)}) = \xi_{i_d}(\gamma_d^{(i_d)},\gamma_d^{(i_d-1)},\cdots,\gamma_d^{(0)};\gamma_{d+1},\gamma_{d+2},\cdots,\gamma_{\mathrm{D}}), \qquad i_d=0,1,\cdots,\mathrm{N}_d \quad (12)$$

Note that the evaluation of equation (11) requires all the support points in $\{\gamma_1^{(0)},\gamma_1^{(1)},\cdots,\gamma_1^{(\mathrm{N}_1)}\}\times\{\gamma_2^{(0)},\gamma_2^{(1)},\cdots,\gamma_2^{(\mathrm{N}_2)}\}\times\cdots\times\{\gamma_{\mathrm{D}}^{(0)},\gamma_{\mathrm{D}}^{(1)},\cdots,\gamma_{\mathrm{D}}^{(\mathrm{N}_{\mathrm{D}})}\}$, as assumed at the start of this section. This constriction of a rectangular grid of support points, which is an inherent characteristic of BCFs, is not suited for an adaptive sampling algorithm that requires the freedom to choose arbitrary support points in the interpolation space. Furthermore, it is expected that a number of the support points in the grid are redundant. This point marks the end of the exposition of standard branched continued fractions.

An important step to enable an adaptive scheme to be applied can now be taken. The constriction of the rectangular grid is removed by approximating certain function values with the previously determined interpolants for those functions when evaluating the function $\xi_{i_d}(\gamma_d^{(i_d)},\gamma_d^{(i_d-1)},\cdots,\gamma_d^{(0)};\gamma_{d+1},\gamma_{d+2},\cdots,\gamma_{\mathrm{D}})$. Equation (11), for $d=1,2,\cdots,\mathrm{D}-1$, therefore becomes

$$\zeta_0(\gamma_d^{(i)};\gamma_{d+1},\gamma_{d+2},\cdots,\gamma_{\mathrm{D}}) \equiv \mathrm{S}(\gamma_1^{(i_1)},\gamma_2^{(i_2)},\cdots,\gamma_d^{(i)},\gamma_{d+1},\cdots,\gamma_{\mathrm{D}}),$$

$$\zeta_1(\gamma_d^{(i)},\gamma_d^{(0)};\gamma_{d+1},\gamma_{d+2},\cdots,\gamma_{\mathrm{D}}) \equiv \frac{\gamma_d^{(i)}-\gamma_d^{(0)}}{\zeta_0(\gamma_d^{(i)};\gamma_{d+1},\gamma_{d+2},\cdots,\gamma_{\mathrm{D}})-\Re_0(\gamma_{d+1},\gamma_{d+2},\cdots,\gamma_{\mathrm{D}}\,|\,\gamma_1^{(i_1)},\gamma_2^{(i_2)},\cdots,\gamma_d^{(0)})},$$
$$i=1,2,\cdots,\mathrm{N}_d \quad (13)$$

$$\zeta_k(\gamma_d^{(i)},\gamma_d^{(k-1)},\cdots,\gamma_d^{(0)};\gamma_{d+1},\gamma_{d+2},\cdots,\gamma_{\mathrm{D}}) \equiv$$
$$\frac{\gamma_d^{(i)}-\gamma_d^{(k-1)}}{\zeta_{k-1}(\gamma_d^{(i)},\gamma_d^{(k-2)},\cdots,\gamma_d^{(0)};\gamma_{d+1},\gamma_{d+2},\cdots,\gamma_{\mathrm{D}})-\Re_{k-1}(\gamma_{d+1},\gamma_{d+2},\cdots,\gamma_{\mathrm{D}}\,|\,\gamma_1^{(i_1)},\gamma_2^{(i_2)},\cdots,\gamma_d^{(k-1)})},$$
$$i=k,k+1,\cdots,\mathrm{N}_d;\ k=2,3,\cdots,\mathrm{N}_d,$$

and equation (12) becomes

$$\Re_{i_d}(\gamma_{d+1}, \gamma_{d+2}, \cdots, \gamma_{\mathrm{D}} \mid \gamma_1^{(i_1)}, \gamma_2^{(i_2)}, \cdots, \gamma_d^{(i_d)}) = \zeta_{i_d}(\gamma_d^{(i_d)}, \gamma_d^{(i_d-1)}, \cdots, \gamma_d^{(0)}; \gamma_{d+1}, \gamma_{d+2}, \cdots, \gamma_{\mathrm{D}}), \qquad i_d = 0, 1, \cdots, \mathrm{N}_d. \quad (14)$$

This simple procedure allows the rectangularly spaced support points required by the BCF to effectively be calculated from mathematical functions constructed from non-rectangularly spaced support points. A few important points should be noted.

(i) Since the number of support points for each univariate function may be different according to equation (13), the orders of the BCFs, N_d, for $d = 2, 3, \cdots, \mathrm{D}$ are now functions of their positions, i.e. $\mathrm{N}_d^{(i_1, i_2, \cdots, i_{d-1})}$, and for implementation, equations (8), (9), (10), (13) and (14) need to be adapted.

(ii) Since each multivariate interpolant is the construct of a set of lower dimensional interpolants, it is important to ensure that the accuracy of these lower dimensional interpolants increases as the number of variables decreases.

(iii) The degree sets of the numerator and the denominator polynomials are completely determined by the form of the BCF, which in turn is determined by the structure of the support points.

(iv) Different numberings of the support points produces different interpolants with dissimilar accuracies [16]. Interpolants are more accurate when the support points are renumbered so that the orders of the BCFs decrease for increasing branches of the BCF.

CHAPTER 3: ADAPTIVE SAMPLING ALGORITHMS

The determination of an accurate rational interpolant $\Re(\gamma)$ requires that enough support points, in the case of microwave circuits, normally CEM analyses, be used. In order to calculate the minimum number and the optimal positions of these support points, an adaptive sampling algorithm is proposed for application to the rational function approximation. In section 3.1 the adaptive sampling algorithm for univariate models with a single output parameter is given. The theory is extended in section 3.2 to allow multivariate sampling and in section 3.3 the formulation is given for multiple output models.

3.1 Univariate Adaptive Sampling

A natural residual term emerges from the univariate rational interpolation formulation as $E_k(\gamma) = \frac{|\Re_k(\gamma) - \Re_{k-1}(\gamma)|^2}{(1+|\Re_k(\gamma)|)^2}$, which provides an estimate of the interpolation error. This is the relative squared error between the current estimate of the interpolant and the previous estimate of the interpolant i.e. before adding the last support point. The residual decreases as k (or the degree of freedom of the function) increases and is zero at $k-1$ support points. The interpolation method formulated in chapter 2 is suitable for an adaptive sampling algorithm, since it produces an error estimate in a very natural way, and it works for unequally spaced support points.

The adaptive algorithm is defined to work in the interval $[\gamma^{(0)}, \gamma^{(1)}]$. As a first step, an arbitrary third support point $\gamma^{(2)}$ is selected which lies in the interval $[\gamma^{(0)}, \gamma^{(1)}]$. This point is required since the residual $E_1(\gamma)$ cannot produce an appropriate error estimate. The coefficient φ_1 for $\Re_1(\gamma)$ is determined from the support points $(\gamma^{(0)}, S_0)$ and $(\gamma^{(2)}, S_2)$, while φ_2 for $\Re_2(\gamma)$ is recursively updated using equation (3) and the support point $(\gamma^{(1)}, S_1)$. The values for S_k at the points $\gamma^{(k)}$ are determined by a CEM analysis. Define I_2 as the interval $[\gamma^{(0)}, \gamma^{(2)}]$. The residual $E_2(\gamma)$ is evaluated at a large number of equi-spaced sample points in the interval I_2 using equation (4). At the maximum of the evaluated sample points a new support point $\gamma^{(3)}$ is selected.

For iteration k the characteristic equation is evaluated at $\gamma^{(k)}$ in order to determine S_k. Equation (3) calculates φ_k recursively. The residual $E_k(\gamma)$ is determined recursively at a large number of equi-spaced sample points on the interval I_k by using equation (4). Assuming the last support point $(\gamma^{(k)}, S_k)$ was selected in the interval $[\gamma^{(i)}, \gamma^{(j)}]$, I_k is defined as both the intervals $[\gamma^{(0)}, \gamma^{(i)}]$ and $[\gamma^{(j)}, \gamma^{(1)}]$. The interval $[\gamma^{(i)}, \gamma^{(j)}]$ is excluded since it does not provide a suitable error estimate. This interval's size generally decreases as the number of support points increases and it varies on alternate iterations. At the maximum of the evaluated residual a new support point $(\gamma^{(k+1)}, S_{k+1})$ is

chosen, thereby minimizing the residual. The process is repeated until the residual becomes arbitrarily small. Fig. 1 shows a step in the execution of the algorithm, with the new sample point indicated with an asterisk. It is important to note that for a full iteration, only one point is determined via a CEM analysis. As all the other computation steps only require the evaluation of the interpolation function, the computational effort is decreased substantially.

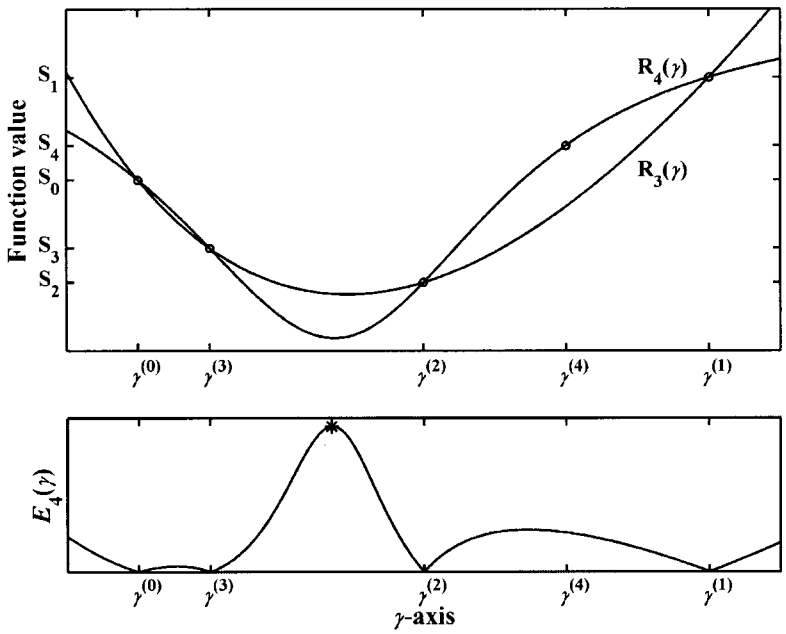

Fig. 1. Illustration of the univariate adaptive sampling technique. The interpolants $\Re_3(\gamma)$, $\Re_4(\gamma)$ and the residual $E_4(\gamma)$ are shown. The asterisk indicates the new support point.

The adaptive sampling algorithm automatically selects and minimises the number of support points, and it does not require any *a priori* knowledge of the dynamics of the function in order to define an interpolation model $\Re(\gamma)$. A few important points should be noted.

(i) The number of equi-spaced evaluations of the residual is not crucial, as long as it is of an order larger than the number of support points. Placing the support points precisely at the successive maxima of the residuals may sometimes slightly decrease the number of support points of the final model. However, the determination of such points through an iterative search algorithm is computationally expensive.

(ii) For highly non-linear functions over the parameter space of interest, the number of support points can become large, causing the order of the rational polynomial to become large and the algorithm to become numerically unstable. Therefore, the number of support points automatically selected by the adaptive sampling algorithm is limited to N_{bd}. If the sampling algorithm has not converged when this limit is reached, the support points in that interval are

sorted in ascending order and subdivided into two new intervals. Each interval is initialised with ½(N_{bd}+1) support points if N_{bd} is odd, or ½N_{bd}+1 and ½N_{bd} support points otherwise. The support point at the cut is used as the last support point in the first interval and also as the first support point in the second interval. Hence all previously determined support points are reused, and more support points will be placed where needed. The intervals become smaller where the errors are larger. The adaptive sampling algorithm is repeatedly applied to each subdivided interval until the interpolant for each interval has attained convergence. The result is a set of interpolants each defined on a specific interval of the complete band that is being modelled. Decreasing N_{bd} produces a more accurate model at the expense of an increased number of interpolants, an increased number of support points and increased computation time.

(iii) Equi-ripple error can only be achieved if the function is known, in which case economisation [12], or specifically a Remes-type algorithm [43] can be used.

(iv) As the accuracy of the model is required to increase, the accuracy of the CEM analysis technique needs to increase. Otherwise, the interpolation process will try to model the error of the CEM analysis and this will lead to an excessive number of support points being selected.

3.2 Multivariate Adaptive Sampling

The multivariate rational interpolation formulation given in section 2.2 is essentially univariate in nature. Therefore, an adaptive sampling algorithm can be applied that is similar to that used for the univariate case. Two different adaptive sampling algorithms are considered. The first algorithm, based on equations (11) and (12), determines a set of support points in the interpolation space placed on a fully filled, not necessarily equispaced, rectangular grid. The second algorithm places support points on a non-rectangular grid and is based on equations (13) and (14). The interpolation space is defined in $\gamma_d \in [\gamma_d^{(0)}, \gamma_d^{(1)}]$ for $d = 1, 2, \cdots, D$. At initialisation an arbitrary set of points $\gamma_d^{(2)}$ are selected in the intervals $[\gamma_d^{(0)}, \gamma_d^{(1)}]$.

An estimate of the interpolation error for the partial interpolants of equation (9) is given in equation (15).

$$E_k(\gamma_d, \gamma_{d+1}, \cdots, \gamma_D \mid \gamma_1^{(i_1)}, \gamma_2^{(i_2)}, \cdots, \gamma_{d-1}^{(k)}) = \frac{\left|\Re_k(\gamma_d, \gamma_{d+1}, \cdots, \gamma_D \mid \gamma_1^{(i_1)}, \gamma_2^{(i_2)}, \cdots, \gamma_{d-1}^{(k)}) - \Re_{k-1}(\gamma_d, \gamma_{d+1}, \cdots, \gamma_D \mid \gamma_1^{(i_1)}, \gamma_2^{(i_2)}, \cdots, \gamma_{d-1}^{(k-1)})\right|^2}{(1+\left|\Re_k(\gamma_d, \gamma_{d+1}, \cdots, \gamma_D \mid \gamma_1^{(i_1)}, \gamma_2^{(i_2)}, \cdots, \gamma_{d-1}^{(k)})\right|)^2} \quad (15)$$

The function $E_k(\gamma_d, \gamma_{d+1}, \cdots, \gamma_D \,|\, \gamma_1^{(i_1)}, \gamma_2^{(i_2)}, \cdots, \gamma_{d-1}^{(k)})$ is defined for the variable γ_d, with $\gamma_{d+1}, \gamma_{d+2}, \cdots, \gamma_D$ defining the position at which the error function can be evaluated. To reduce the computational effort required in evaluating equation (15), especially for a larger number of variables, $E_k(\gamma_d, \gamma_{d+1}, \cdots, \gamma_D \,|\, \gamma_1^{(i_1)}, \gamma_2^{(i_2)}, \cdots, \gamma_{d-1}^{(k)})$ is only evaluated at $\gamma_{d+1}=\gamma_{d+1}^{(2)}$, $\gamma_{d+2}=\gamma_{d+2}^{(2)}, \cdots, \gamma_D=\gamma_D^{(2)}$. Practical examples have shown that $E_k(\gamma_d, \gamma_{d+1}, \cdots, \gamma_D \,|\, \gamma_1^{(i_1)}, \gamma_2^{(i_2)}, \cdots, \gamma_{d-1}^{(k)})$ is largely independent of the variables $\gamma_{d+1}, \gamma_{d+2}, \cdots, \gamma_D$, provided that $\Re_k(\gamma_d, \gamma_{d+1}, \cdots, \gamma_D \,|\, \gamma_1^{(i_1)}, \gamma_2^{(i_2)}, \cdots, \gamma_{d-1}^{(k)})$ is accurate for all k. Due to the renumbering of the support points, as mentioned in section 2.2, it is necessary that an error function be zero at all of the support points in order to be able to place a new support point at the maximum of this error function. Evaluation of the error function in equation (15), with the support points in the series $\{\gamma_d^{(0)}, \gamma_d^{(1)}, \cdots, \gamma_d^{(N_d)}\}$, will determine a function which is zero at all of the support points except at $\gamma_d^{(N_d)}$. A different error function can be defined, which is zero at all of the support points except at $\gamma_d^{(N_d-1)}$, when the last two support points in the series are swapped around. A new error function, defined as the product of the square root of the above two error functions, is zero at all of the support points. Although the same method can be applied to the univariate case, this has no benefit.

The first multivariate adaptive sampling algorithm, denoted **ASA1**, constructs the multivariate rational interpolant as follows:

1. Using the univariate adaptive sampling algorithm, construct a univariate model of each variable γ_d over the interval $[\gamma_d^{(0)}, \gamma_d^{(1)}]$, with all other variables set to their midpoint values, i.e. $\gamma_m = \gamma_m^{(0)} + \frac{1}{2}(\gamma_m^{(1)} - \gamma_m^{(0)})$ for $m = 1, 2, \cdots, D$ and $m \neq d$. In this way, D univariate interpolants and their respective sets of support points, each lying on a line crossing through the centre of the interpolation space, are established.
2. Sort the variable positions, d, in the multivariate interpolant $\Re(\gamma_1, \gamma_2, \cdots, \gamma_D)$ so that the orders N_d of the interpolants determined in step 1 decrease as d increases.
3. Generate a rectangular grid of support points from the points determined in step 1, i.e. all the points in $\{\gamma_1^{(0)}, \gamma_1^{(1)}, \cdots, \gamma_1^{(N_1)}\} \times \{\gamma_2^{(0)}, \gamma_2^{(1)}, \cdots, \gamma_2^{(N_2)}\} \times \cdots \times \{\gamma_D^{(0)}, \gamma_D^{(1)}, \cdots, \gamma_D^{(N_D)}\}$.
4. Create a multivariate rational interpolant from the grid of support points defined in step 3 using equations (11), (12) and (3).

ASA1 is expounded by means of a bivariate example exemplified in Fig. 2. Step 1 of the algorithm determines the star-shaped support points by means of a univariate interpolation along the dimensions γ_1 and γ_2 at $\gamma_2^{(2)}$ and $\gamma_1^{(2)}$ respectively. Since $N_1 = 6$ is smaller than $N_2 = 7$ in the example, γ_1 and γ_2 are exchanged in the interpolant. Hence, the interpolant $\Re(\gamma_2, \gamma_1)$ consists of a union of univariate interpolants $\Re(\gamma_1)$. In step 3 a grid of support points is generated by adding the circle-shaped support points as shown in Fig. 2. $\Re(\gamma_2, \gamma_1)$ is created from this rectangular grid of

support points.

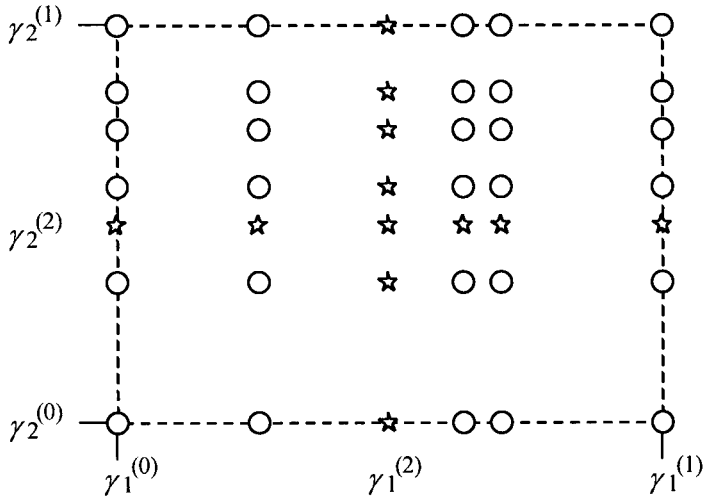

Fig. 2. Illustration of the support point placement using ASA1.

The second multivariate adaptive sampling algorithm, denoted **ASA2**, constructs the multivariate rational interpolant as follows:

1. Same as for ASA1.
2. Same as for ASA1.
3. Initialise a model with a rectangular grid of support points with three support points along every dimension, i.e. 3^D support points in $\{\gamma_1^{(0)},\gamma_1^{(1)},\gamma_1^{(2)}\}\times\{\gamma_2^{(0)},\gamma_2^{(1)},\gamma_2^{(2)}\}\times\cdots\times\{\gamma_D^{(0)},\gamma_D^{(1)},\gamma_D^{(2)}\}$.
4. Construct a multivariate rational interpolant from the support points using equations (13), (14) and (3).
5. Select a dimension γ_d for selection of new support points. Iterate for $d=D, D-1, \cdots, 1$.
6. Select new support points at the maxima of the error function, equation (15), at positions along γ_d.
7. Renumber the support points so that $N_d^{(i_1,i_2,\cdots,i_{d-1})}$ decrease as the numberings i_d increases.
8. Repeat steps 4 thru 8 until convergence.

ASA2 is expounded by means of a bivariate example illustrated in Fig. 3. Step 1 and step 2 are the same as in ASA1. Assume N_2 is smaller than N_1. In step 3 an initialisation grid of 9 support points is generated as shown by the star-shaped support points in Fig. 3(a). $\Re(\gamma_1,\gamma_2)$ is created from these 9 support points. Using the univariate adaptive sampling algorithm $\Re_0(\gamma_2\,|\,\gamma_1^{(0)})$ is completely determined with a predefined accuracy by placing support points at $\gamma_1^{(0)}$. Then $\Re_1(\gamma_2\,|\,\gamma_1^{(1)})$ is determined at $\gamma_1^{(1)}$. Since $N_2^{(0)}=7$ is bigger than $N_2^{(1)}=6$, the algorithm continues by determining $\Re_2(\gamma_2\,|\,\gamma_1^{(2)})$ at $\gamma_1^{(2)}$. With $N_2^{(2)}=8$, the support points are renumbered so that the support points at

$\gamma_1^{(2)}$ determine $\Re_0$, the support points at $\gamma_1^{(0)}$ determine $\Re_1$ and the support points at $\gamma_1^{(1)}$ determine $\Re_2$ in equation (7), and hence $\gamma_1^{(0)},\gamma_1^{(1)},\gamma_1^{(2)}$ become $\gamma_1^{(1)},\gamma_1^{(2)},\gamma_1^{(0)}$ respectively, as shown in Fig. 3(b). Then the error function is evaluated for γ_1 at $\gamma_2^{(2)}$ and $\gamma_1^{(3)}$ is determined at the maximum of this error. $\Re_3(\gamma_2 \mid \gamma_1^{(3)})$ is initialised with three support points at $\gamma_2^{(0)}$, $\gamma_2^{(1)}$ and $\gamma_2^{(2)}$, shown by the star-shaped support points in Fig. 3(b). Using the univariate adaptive sampling algorithm $\Re_3(\gamma_2 \mid \gamma_1^{(3)})$ is completely determined at $\gamma_1^{(3)}$. The process is repeated until the error function has reached its required accuracy.

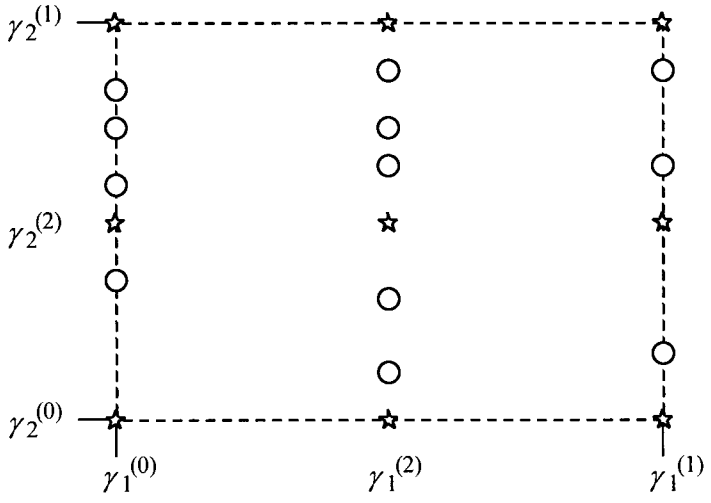

(a)

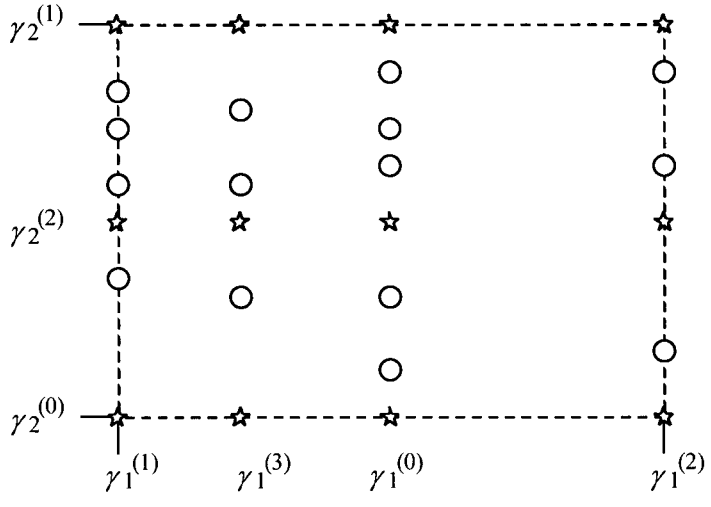

(b)

Fig. 3. Illustration of the support point placement using ASA2. (a) After three steps. (b) After the fourth step.

If required, interval subdivision as mentioned in section 3.1 for the univariate case is applied to the variable γ_D.

3.3 Multiple output interpolation models

For the modelling of functions with more than one complex numbered output parameter, i.e. $S_{i_1,i_2,\cdots,i_D}$ being multi-dimensional complex numbered vectors, the model $\Re(\gamma_1,\gamma_2,\cdots,\gamma_D)$ consists of a set of interpolants, where each interpolant models one of the output parameters. Hence,

$$\Re(\gamma_1,\gamma_2,\cdots,\gamma_D)=[\Re^{(1)}(\gamma_1,\gamma_2,\cdots,\gamma_D),\Re^{(2)}(\gamma_1,\gamma_2,\cdots,\gamma_D),\cdots,\Re^{(E)}(\gamma_1,\gamma_2,\cdots,\gamma_D)], \tag{16}$$

where $\Re^{(e)}(\gamma_1,\gamma_2,\cdots,\gamma_D)$, $e=1,2,\cdots,E$, are interpolants that model entries in the E-dimensional output vector.

A CEM analysis generally produces all the output parameters, usually scattering parameters, with little more effort than it needs to determine one output parameter. In order to select the support points for the model $\Re(\gamma_1,\gamma_2,\cdots,\gamma_D)$ efficiently in the parameter space, the same set of support points are selected for all of the interpolants $\Re^{(e)}(\gamma)$, $e=1,2,\cdots,E$. This will lead to a reduction in the total number of CEM analyses compared to the case where separate sets of support points are determined for each interpolant.

The basis of this technique lies in the definition of a global error function incorporating all the output parameters. Define an error function as:

$$E_k(\gamma_d,\gamma_{d+1},\cdots,\gamma_D\,|\,\gamma_1^{(i_1)},\gamma_2^{(i_2)},\cdots,\gamma_{d-1}^{(k)})=\max_e\left[E_k^{(e)}(\gamma_d,\gamma_{d+1},\cdots,\gamma_D\,|\,\gamma_1^{(i_1)},\gamma_2^{(i_2)},\cdots,\gamma_{d-1}^{(k)})\right],\qquad e=1,2,\cdots,E. \tag{17}$$

The error function $E_k^{(e)}(\gamma_d,\gamma_{d+1},\cdots,\gamma_D\,|\,\gamma_1^{(i_1)},\gamma_2^{(i_2)},\cdots,\gamma_{d-1}^{(k)})$, which is the error of each individual interpolant, was defined in section 3.2 and is zero at all of the support points.

The adaptive sampling algorithm for the multiple output interpolation models, denoted **ASA3**, is identical to ASA2 defined in section 3.2 with the difference that the error function in equation (17) is used and new support points are placed at the maxima of this error function. Therefore all the error functions of the individual interpolants are taken into account when selecting a new support point.

CHAPTER 4: RESULTS – UNIVARIATE ADAPTIVE SAMPLING

In this chapter the results are shown for two applications of the univariate adaptive sampling algorithm. Firstly, it was implemented into an aggressive space mapping optimisation technique for the design of a rectangular waveguide filter with capacitive step discontinuities [31]. Secondly, it was applied to the calculation of transmission line characteristics by the two-dimensional Method-of-Lines of two- and three-layer shielded planar structures [32].

4.1 Rectangular waveguide filter with capacitive step discontinuities

Aggressive space mapping (ASM) is well-known as a technique to optimise a microwave circuit using the minimum number of fine model (CEM) simulations and transferring the bulk of CPU intensive optimisation to the coarse model (empirical circuit-theoretic model) parameter space [44], [45]. The ASM technique iteratively establishes a mapping between the spaces of the design parameters of the two models. Define the vectors $\mathbf{x}_{os}$ and $\mathbf{x}_{em}$ as the design parameters of the coarse and the fine models respectively, and $\mathbf{R}_{os}(\mathbf{x}_{os})$ and $\mathbf{R}_{em}(\mathbf{x}_{em})$ as the corresponding model responses. Parameter extraction is used to determine $\mathbf{x}_{os}$, whose response matches the fine model response at $\mathbf{x}_{em}$ for every space mapping iteration. A brief review of ASM is given in Appendix A.

The number of frequency points used to do the parameter extraction in the ASM technique is usually chosen arbitrarily. It is important that this number be kept as small as possible to minimise the CEM evaluation time. However, choosing this number too small can cause the parameter extraction procedure to fail, which in turn causes the ASM algorithm to converge slowly, oscillate or even diverge [46]. Failure of the whole ASM procedure may result if the parameter extraction is not unique, falls into a local minimum due to severe response misalignment at initialisation, or if the coarse model cannot adequately model the fine model response. Normally, the way to guarantee good parameter extraction is to use a sufficiently large number of frequency points. The integration of the univariate adaptive sampling algorithm into the ASM optimisation ensures that for every ASM iteration (i) the number of CEM analyses are minimised and (ii) enough frequency points can be used for the parameter extraction.

The adaptive sampling algorithm creates the model $\Re(f|\mathbf{x}_{em})$ with the minimum number of frequency support points. $\Re(f|\mathbf{x}_{em})$ is an approximation of the fine model response $\mathbf{R}_{em}(\mathbf{x}_{em})$, which is valid for the parameter vector $\mathbf{x}_{em}$ over the desired interpolation interval. Given $\Re(f|\mathbf{x}_{em})$, an arbitrarily large number of frequency points can be chosen to ensure the non-failure of the parameter extraction step. Note that the ASM technique combined with the adaptive sampling

algorithm requires the convergence of three iterative processes, namely (i) adaptive sampling to establish $\Re(f|\mathbf{x}_{em})$; (ii) parameter extraction to determine $\mathbf{x}_{os}$, whose response matches $\Re(f|\mathbf{x}_{em})$; and (iii) space mapping to find $\mathbf{x}_{em}$ that produces the optimal response according to design specifications.

The design of a rectangular waveguide filter with eight capacitive steps as shown in Fig. 4 is considered. The design specification for the filter is a reflection coefficient $|S_{11}| \leq -25$ dB in the range [9 GHz, 11 GHz]. The design is for a standard WR90 rectangular waveguide and the capacitive step lengths are all chosen to be 2 mm. The filter is symmetric with eight optimisation variables (L_1, L_2, L_3, L_4, C_1, C_2, C_3, C_4) as defined by the coarse (transmission line) model in Fig. 4(a). The fine model is a mode-matching solution combined with the generalised scattering matrix [47]. The parameter extraction optimisations are driven by a BFGS quasi-Newton method with a mixed quadratic and cubic line search procedure [48]. ℓ_1 norm objectives are used throughout the ASM algorithm. The input parameter $\mathbf{x}_{os}^*$, which produces the optimal response, is determined by a minimax optimisation on the coarse model, also using the BFGS quasi-Newton method. The response $\mathbf{R}_{os}(\mathbf{x}_{os}^*)$ is shown in Fig. 5 (dotted line).

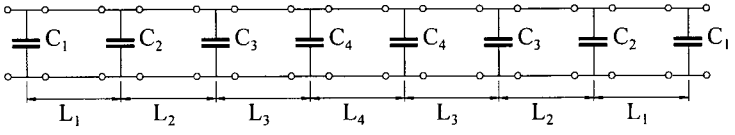

(a)

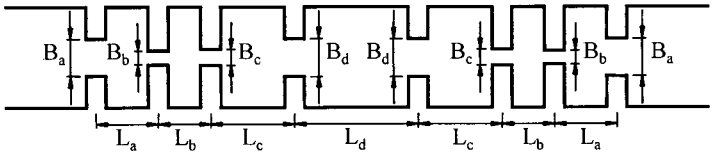

(b)

Fig. 4. The coarse model (a) and the physical structure (b) of the rectangular waveguide filter with capacitive step discontinuities.

Standard ASM assumes that $\mathbf{x}_{os}$ and $\mathbf{x}_{em}$ describe the same physical parameters, which is not the case here. The capacitance and the transmission line length for a waveguide step can be calculated using the mode-matching technique for several values of the gap opening. Interpolation of these values establishes a mapping from the circuit model variables $\mathbf{x}_{em}$ to the physical waveguide dimensions. Since the ASM technique compares $\mathbf{R}_{os}(\mathbf{x}_{os})$ and $\mathbf{R}_{em}(\mathbf{x}_{em})$ this mapping is incorporated into the ASM.

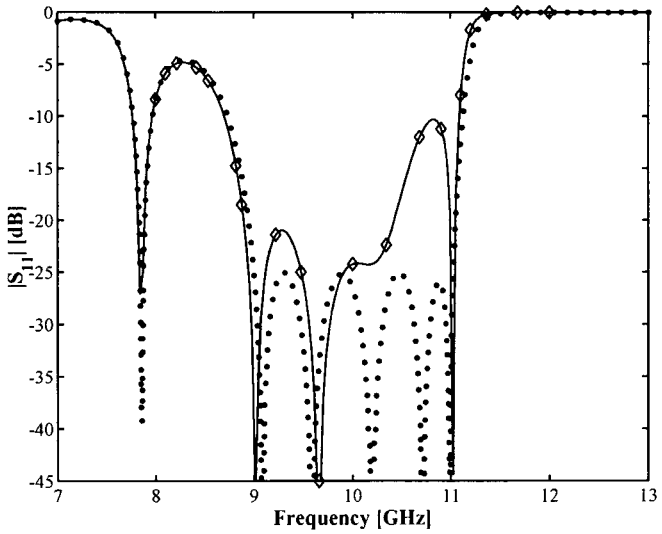

Fig. 5. Response $\Re(f|\,\mathbf{x}_{em})$ (solid line) at initialisation with 19 support points (diamonds) and the optimal response (dotted line). Support points smaller than –45 dB are shown at –45 dB.

Table 1. Convergence of $\Re(f|\,\mathbf{x}_{em})$ determined by the univariate adaptive sampling algorithm.

		$\lvert\Re_k(f\mid \mathbf{x}_{em})-\Re_{k-1}(f\mid \mathbf{x}_{em})\rvert$ [dB]	
k	Support points [GHz]	Mean	Max
3	[8, 10, 12]	– 20.0	– 5.4
4	9.22	– 16.0	– 1.6
5	11.10	– 16.7	30.3
6	9.66	– 18.7	10.6
7	8.82	– 23.9	– 16.1
8	11.68	– 22.1	3.7
9	8.88	– 4.5	10.3
10	11.20	– 10.0	– 0.9
11	8.42	– 5.3	34.0
12	10.34	– 24.4	13.9
13	9.48	– 26.4	– 11.2
14	11.36	– 35.1	– 11.1
15	10.90	– 42.3	– 34.2
16	8.22	– 29.7	– 28.4
17	8.54	– 41.6	– 29.7
18	8.10	– 59.1	– 34.7
19	10.68	– 89.2	– 42.9

As a first step a univariate model $\Re(f|\,\mathbf{x}_{em}^{(1)})$ with $\mathbf{x}_{em}^{(1)} = \mathbf{x}_{os}^{*}$ was created with the adaptive sampling algorithm for the reflection coefficient S_{11}. The interpolation interval is defined for $f \in [8\,\text{GHz}, 12\,\text{GHz}]$ and the initial support points were chosen at 8 GHz, 10 GHz (arbitrary) and 12 GHz. The convergence of the adaptive sampling algorithm is shown in Table 1. After several iterations, i.e. when the order of the interpolation polynomial is sufficiently large to model the response adequately, the residual converges very quickly. Convergence was assumed when the maximum absolute error between the current estimate of the interpolant and the previous estimate of the interpolant was smaller than –40 dB. The absolute error was evaluated at 500 equi-spaced points over the interpolation interval. Fig. 5 (solid line) shows the response of the model $\Re(f|\,\mathbf{x}_{em}^{(1)})$ with only 19 support points (diamonds). The fine and the coarse model responses differ significantly due to the evanescent modes coupling between capacitive steps.

For the parameter extraction step 30 frequency points equally spaced over the frequency band were used. The ASM optimisation converged to the solution within 2 iterations. The result is shown in Fig. 6. Table 2 and Table 3 show $\mathbf{x}_{os}$ and $\mathbf{x}_{em}$ respectively after every ASM iteration. Table 4 lists $\mathbf{x}_{em}$ transformed to the physical waveguide dimensions (Fig. 4(b)). The adaptive sampling algorithm converged with 19, 19 and 20 iterations for every ASM iteration. Therefore, in total 58 CEM evaluations were required.

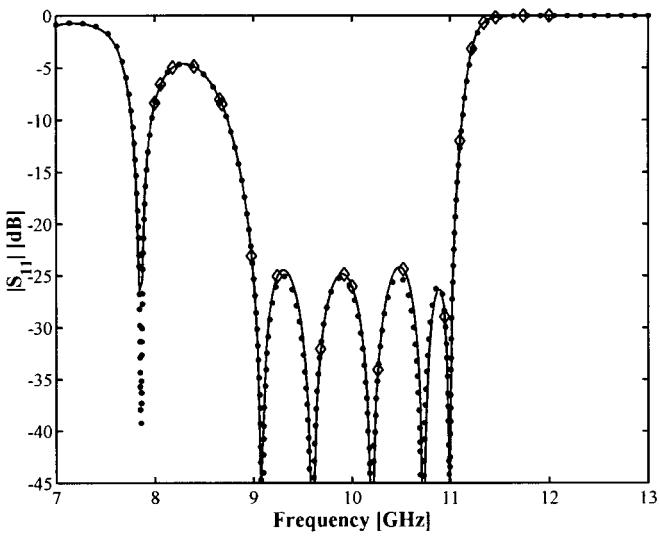

Fig. 6. Response $\Re(f \mid \mathbf{x}_{em})$ (solid line) after the second ASM iteration with 20 support points (diamonds) and the optimal response (dotted line).

Table 2. ASM iterations of the coarse model.

Parameter	$\mathbf{x}_{os}^{(1)}$	$\mathbf{x}_{os}^{(2)}$	$\mathbf{x}_{os}^{(3)}$
C_1	20.332	21.262	20.911
C_2	65.196	65.631	64.257
C_3	54.559	55.316	54.138
C_4	20.783	21.326	21.014
L_1	44.434	42.772	43.259
L_2	33.380	31.783	32.366
L_3	62.340	61.224	62.152
L_4	100.474	100.194	100.580
Capacitance values in pF, length values in degrees relative to 10 GHz			

Table 3. ASM iterations of the fine model.

Parameter	$\mathbf{x}_{em}^{(1)}$	$\mathbf{x}_{em}^{(2)}$	$\mathbf{x}_{em}^{(3)}$
C_1	20.911	21.490	21.119
C_2	64.257	63.318	61.865
C_3	54.138	53.717	52.472
C_4	21.014	21.245	20.915
L_1	43.259	42.084	42.599
L_2	32.366	31.351	31.968
L_3	62.152	61.964	62.945
L_4	100.580	100.686	101.093
Capacitance values in pF, length values in degrees relative to 10 GHz			

Table 4. ASM iterations of the fine model physical dimensions.

Parameter	$\mathbf{x}_{em}^{(1)}$	$\mathbf{x}_{em}^{(2)}$	$\mathbf{x}_{em}^{(3)}$
B_a	3.8608	3.7844	3.8332
B_b	1.2875	1.3099	1.3457
B_c	1.5702	1.5842	1.6271
B_d	3.8471	3.8165	3.8602
L_a	6.2494	6.1251	6.1734
L_b	5.2796	5.1640	5.2240
L_c	8.3058	8.2867	8.3862
L_d	12.3140	12.3318	12.3680
All values in mm			

The design was repeated using the ASM algorithm without the adaptive sampling algorithm with the number of equally spaced frequencies N_s for the parameter extraction step set to 19. The parameter extraction did not properly align the two responses at initialisation as shown in Fig. 7 (resonance at about 10.1 GHz should have been at about 11 GHz) causing the ASM algorithm to converge slowly. To compare this with the previous example, the result is shown in Fig. 8 after 2 ASM iterations. It is clear that the ASM is far from achieving convergence. The ASM converged after 8 iterations requiring 171 CEM evaluations. The adaptive sampling algorithm shows a significant improvement over this result.

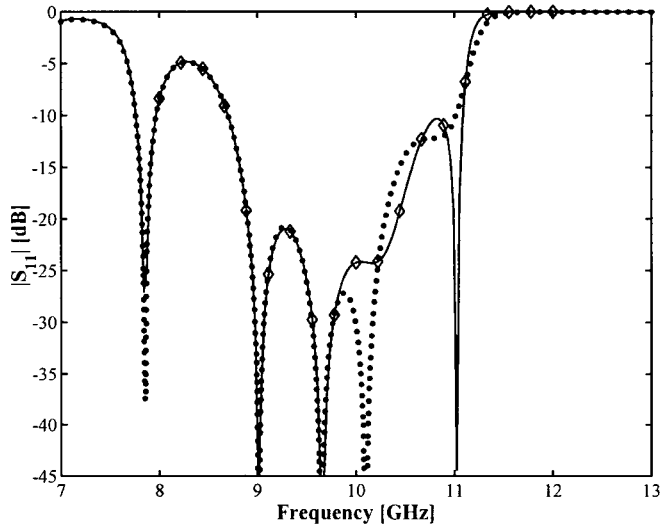

Fig. 7. The fine model response (solid line) and the response determined by the parameter extraction optimisation (dotted line) with 19 equally spaced frequency points (diamonds) at initialisation.

The design was then repeated for various values of N_s. The results are tabulated in Table 5. The ASM error is the sum of the difference between $\mathbf{x}_{os}^{(j)}$ and $\mathbf{x}_{os}^{*}$ normalised with respect to $\mathbf{x}_{os}^{*}$. Failure of convergence is indicated by ∞. With N_s chosen large (70, 50 and 30) the parameter extraction optimisation converged and the ASM algorithm converged quickly. In this case, N_s is proportional to the number of CEM evaluations. Decreasing N_s causes the ASM optimisation to diverge or converge slowly, due to the parameter extraction step falling into local minima.

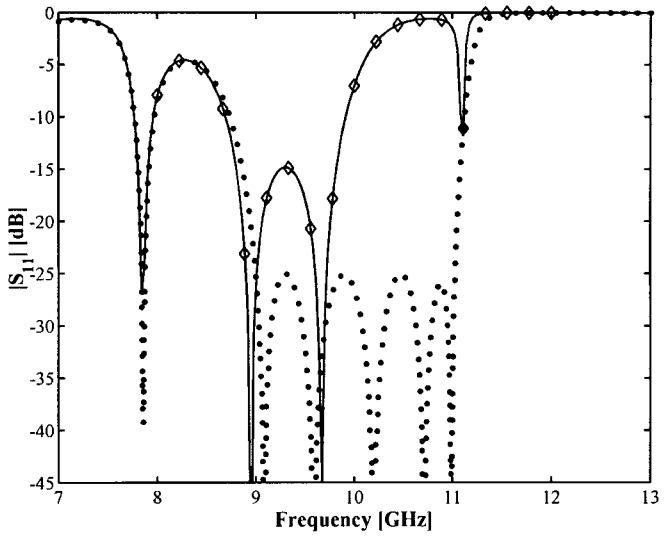

Fig. 8. The fine model response (solid line) after the second ASM iteration with the parameter extraction optimisation using 19 equally spaced frequency points (diamonds). The dotted line represents the optimal response.

Table 5. ASM iterations for various N_s in the parameter extraction step.

Number of frequencies, N_s	ASM error < 10^{-4}		ASM error < 10^{-10}	
	ASM iterations	Number of CEM evaluations	ASM iterations	Number of CEM evaluations
70	2	210	2	210
50	2	150	2	150
30	2	90	3	120
25	∞	∞	∞	∞
23	1	46	9	230
22	∞	∞	∞	∞
19	8	171	8	171
15	5	90	9	150
10	∞	∞	∞	∞

4.2 Modal propagation constants of shielded planar structures

The calculation of the propagation constants of modes in quasi-TEM microwave structures is a well-known problem in literature [49]-[53], and increasingly of interest in hybrid numerical analysis techniques incorporating Mode-Matching [54]-[56]. In the case of shielded planar structures, the two-dimensional Method-of-Lines (MoL) offers a very efficient analysis option, as it involves discretization of the two-dimensional Helmholz equation in only one direction [57]-[60]. This results in a number of coupled differential equations, which are de-coupled using matrix techniques. The result is a number of uncoupled differential equations, each describing a transformed field or potential along a *line* instead of at a single point, hence the name Method-of-Lines. The elimination of discretization in one dimension is the key feature of the MoL and results in reduced computer storage requirements and reduced run-times. The two-dimensional MoL has been shown by numerous authors to be fast, accurate and effective. However, in this method, as in many other formulations, the propagation constants of the modes are calculated by solving the function in

equation (18), a severely non-linear function with an infinite number of solutions, normally interspersed with an infinite number of poles, together with very sharp non-zero local minima. For loss-less problems, the zeros can be purely real, purely imaginary or complex.

$$f(\gamma) = \det[\mathrm{Y}(\gamma)] = 0 \tag{18}$$

As the existence of poles in the equation to be solved creates significant problems for most root-finding algorithms, a number of attempts to find pole-free solutions have been published. These include pole-free formulations [61], the use of a singular-value decomposition method (SVD) [62], and finding the pole-positions analytically and either removing them, as reported in [57], or searching between them [56]. Of these, the SVD method seems to produce the best results, at the cost of creating a function with a discontinuous first derivative, making the use of fast gradient root-finding algorithms difficult.

The adaptive sampling algorithm establishes, with the minimum number of evaluations of the characteristic equation (18), an accurate approximation $\Re(\gamma)$ to the characteristic function $f(\gamma)$. The approximation can be written as the ratio of two polynomials, of which only the pole-free numerator needs to be solved for the zeros of the function according to equation (4). An added advantage of the polynomial representation is that the derivatives of the function can easily be calculated using equation (5), enabling the use of gradient root-finding algorithms. Neither the evaluation of the numerator nor its derivative are computationally expensive. Two sets of models are created, one for the real axis $\Re(\gamma = \alpha)$ and one for the imaginary axis $\Re(\gamma = \mathrm{j}\beta)$ to determine all the propagation constants for both the propagating and evanescent modes respectively. Although it is possible to create a model $\Re(\gamma)$ in the complex γ-plane using the theory of section 2.1, such a model requires a large number of support points in order to achieve the required accuracy. As typical problems exhibit small numbers of zeros in the complex γ-plane, a constrained root finding algorithm is applied directly to the characteristic equation.

A first order Newton-Raphson root-finding method is applied to the models $\Re(\gamma)$ and a bisection search is used when the former failed [63]. The maximum Newton-Raphson step size was limited to 10 % of the search interval. The zero suppression technique [64] is used to prevent the root finding algorithm to converge to the same root twice. It implies that the derivative used in the Newton-Raphson method is changed to:

$$\frac{\partial \mathrm{N}(\gamma)}{\partial \gamma} - \sum_{i=1}^{\mathrm{N}_r} \frac{\mathrm{N}(\gamma)}{\gamma - \xi_i}, \tag{19}$$

where ξ_i are the N_r previously found roots. The advantage of this technique, as opposed to deflation

where the polynomial $N(\gamma)$ is divided by $\gamma-\xi_i$ explicitly so as to give a lower order polynomial, is that the accuracy of a new root is not sensitive to the errors incurred in calculating the previous roots. The root finding algorithm is initialised at the lowest γ value in the interval and forced to search in the positive γ direction until it reaches the highest γ value in the search interval. To ensure that roots on the border of the interval are found, the root finding algorithm is allowed to search past the highest γ value by 1 % of the band.

The accuracy of the models $\Re(\gamma)$ is required to be high to ensure that the root positions of $\Re(\gamma)$ are accurate and that $\Re(\gamma)$ does not miss any roots, which are found in the characteristic equation (18). As described in section 2.1, this demand on accuracy can cause the adaptive sampling algorithm to produce pole/zero combinations, with the result that more zeros are determined than are present in the characteristic equation. We therefore test the validity of all zeros found by the root finding algorithm. If a root is closer than 10^{-3} to a pole, it is eliminated. The poles are found by doing a first order Newton-Raphson search of $D(\gamma)$ in the vicinity of the roots.

The complex conjugate roots, i.e. the complex propagation constants, in the complex γ-plane are found directly from the characteristic equation (18) by using a secant search method, which requires two characteristic equation evaluations per iteration. The search space is divided into a number of areas in the β direction. In each area the search is constrained within that area by dividing the characteristic equation by the following equation

$$(\alpha)(\alpha-\alpha_u)(\beta-\beta_l)(\beta-\beta_u), \tag{20}$$

and limiting the Newton-Raphson step size to fall within this area. α_u is the upper limit on the real axis, and β_l and β_u are respectively the lower and upper limits on the imaginary axis. Since the imaginary part of the complex roots is generally small, the size of the areas is progressively increased further away from the α-axis. The areas were allowed to slightly overlap to ensure that roots on the border are found.

The maximum step size was limited to 20 % of the diagonal of the search area and zero suppression as mentioned above is used. In the α direction the algorithm was started at N_{st} different positions to prevent it from converging to local minima and to allow it to search the whole area. The following starting positions were used:

$$\frac{2i+1}{2N_{st}}\alpha_u + j0.05(\beta_u-\beta_l)+\beta_u, \qquad i=0, 1, \cdots, N_{st}-1 \tag{21}$$

The technique was tested on two examples: a shielded microstrip line structure and a centred slot

unilateral fin line structure. For the adaptive sampling algorithm we limited the maximum order of the rational polynomial in an interval (N_{bd}) to 29. The residual $E_k(\gamma)$ as defined in section 3.1 in an interval was evaluated at 500 points and convergence was assumed when the maximum value of this residual was smaller than −80 dB. For the root finding algorithms the maximum number of iterations allowed until convergence was 30 and convergence was assumed when the step size was smaller than 10^{-5}. For the complex root finding algorithm the number of divisions in the β direction was chosen to be 3 and N_{st} was chosen as 15 (closest to α-axis), 10 and 5 (furthest from α-axis) for the three areas.

4.2.1 Shielded microstrip line

The loss-less shielded microstrip line structure is shown in Fig. 9. The region searched for roots was chosen as $[0, j2.979]$ on the imaginary axis and $[0, 2]$ on the real axis. Only the even order modes were calculated and uniform discretization was used. Table 6 shows the support points selected by the adaptive sampling algorithm after every iteration for the microstrip line at 20 GHz. The propagation constants are normalised with respect to the free space wave number k_0, i.e. $\gamma/k_0 = \alpha/k_0 + j\beta/k_0$. On the real axis the interval was automatically divided into two intervals, α_1 and α_2, when the number of support points reached 29. The shaded areas show the 29 support points before interval division. Both the mean and the maximum relative errors after every iteration, as well as the roots found in each interval are shown.

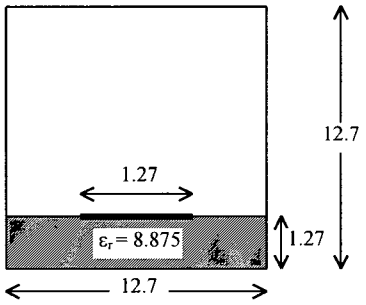

Fig. 9. Cross-section of the shielded microstrip line. All dimensions are given in millimetres.

Fig. 10 shows the interpolation model response and the support points for the model constructed over interval α_2. Fig. 11 shows the residual $E_k(\gamma)$ at convergence of the adaptive sampling algorithm and the relative error between the characteristic equation response and the interpolation model response, i.e. $\frac{|\det[Y(\gamma)] - \Re_k(\gamma)|}{1 + \det[Y(\gamma)]}$. Fig. 12 shows the calculated numerator and denominator polynomials and their respective derivatives of the function given in Fig. 10.

Table 6. Adaptive sampling algorithm iterations for shielded microstrip line (Fig. 9) at 20 GHz. The shaded areas show the support points used for initialisation on the β-axis, and those determined before interval division on the α-axis. Propagation constants are normalised with respect to the free space wave number k_0.

	$j\beta \in [0; j2.979]$			$\alpha_1 \in [0; 1.463]$			$\alpha_2 \in [1.463; 2]$		
	Support	$E_k(\gamma)$ [dB]		Support	$E_k(\gamma)$ [dB]		Support	$E_k(\gamma)$ [dB]	
k	points	Mean	Max	points	Mean	Max	points	Mean	Max
1	0			0			1.463		
2	j1.489			0.136			1.495		
3	j2.979	4.8	41.1	0.497			1.559		
4	j1.110	−22.6	11.8	0.589			1.583		
5	j2.877	−47.9	−34.4	0.625			1.595		
6	j1.098	−11.9	4.5	0.733			1.603		
7	j2.955	−5.0	34.7	1.000			1.623		
8	j2.782	27.2	75.7	1.034			1.876		
9	j1.260	6.3	30.1	1.066			1.940		
10	j2.633	3.0	39.2	1.106			1.956		
11	j0.680	−38.6	−6.6	1.194			1.960		
12	j2.394	−2.7	37.7	1.351			1.968		
13	j0.836	−4.2	35.2	1.367			1.972		
14	j0.573	−19.8	20.5	1.387			1.996		
15	j0.704	−13.4	24.7	1.463	−50.2	−35.6	2.000	−13.9	32.5
16	j0.495	16.7	68.2	0.551	−18.8	25.0	1.828	−1.3	35.9
17	j0.597	−18.9	5.5	0.243	−48.4	−0.9	1.476	3.2	43.2
18	j0.490	−47.8	−0.8	1.460	−67.4	−48.7	1.610	−2.9	40.6
19	j1.904	−6.9	27.5	0.067	−81.9	−62.0	1.756	−64.8	−33.0
20	j0.304	−81.7	−47.0	1.445	−81.5	−65.7	1.601	−54.5	−14.3
21	j0.806	−55.5	−9.9	0.023	−72.4	−55.4	1.792	−84.8	−59.5
22	j0.472	−65.6	−40.3	0.138	−84.7	−70.5	1.751	−40.1	2.3
23	j0.066	−96.0	−53.4	0.334	−104.0	−83.0	1.759	−101.8	−58.6
24	j0.424	−105.0	−67.3				1.794	−139.2	−108.7
25	j1.988	−130.8	−95.9						
Roots found		j0.59457 j0.72511 j1.1027 j2.7106			0.55192			1.4978 1.6102 1.7589 1.8744	

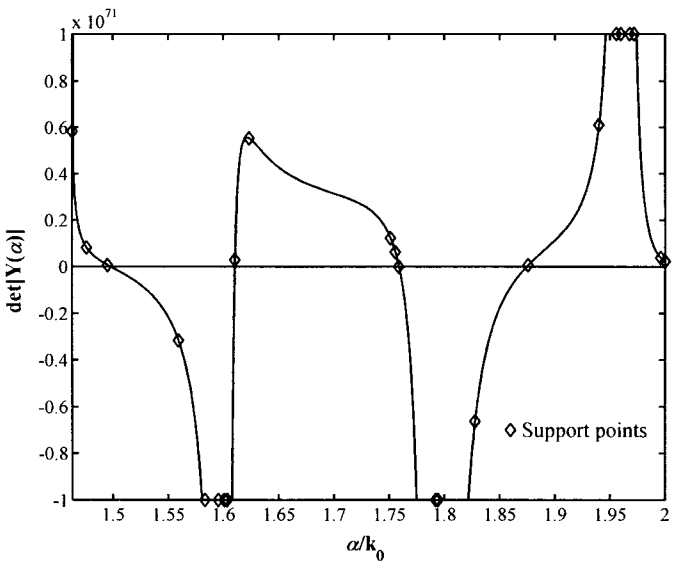

Fig. 10. Response $\Re(\gamma)$ with 25 support points (diamonds) for the structure of Fig. 9 at 20 GHz. This is the second interval, i.e. α_2, on the α-axis as chosen by interval division. Support points larger than $+/-10^{71}$ are shown at $+/-10^{71}$ respectively.

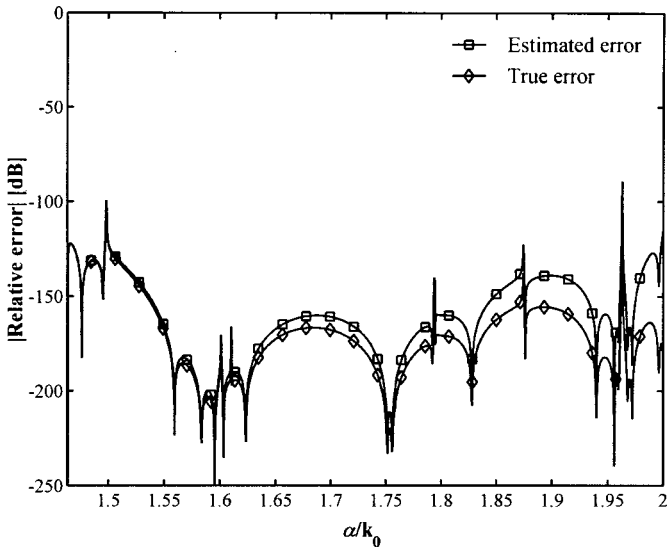

Fig. 11. The relative error estimated by the adaptive sampling algorithm at convergence and the relative error between the characteristic equation response and the interpolation model response (Fig. 10).

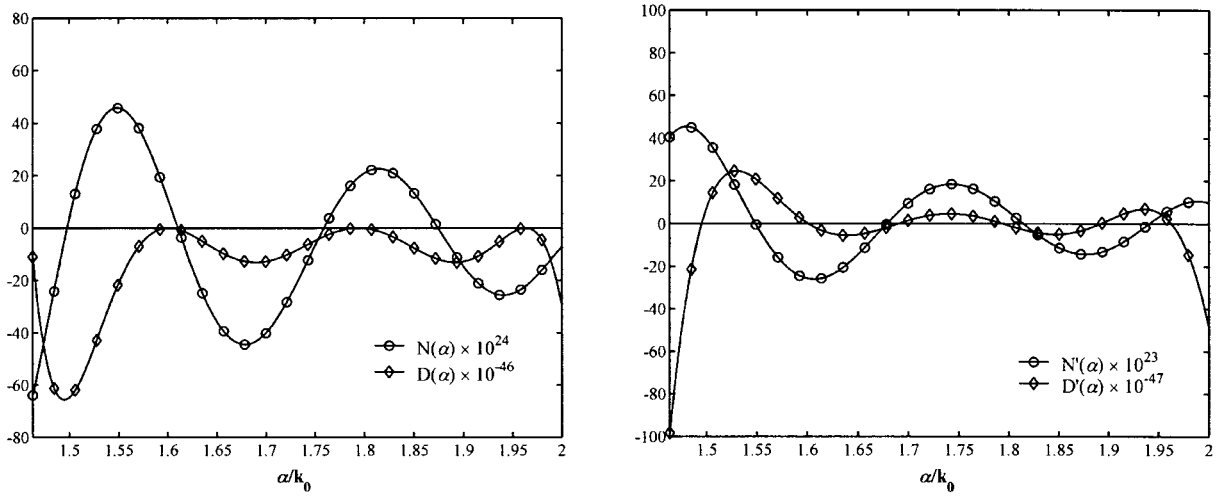

Fig. 12. The interpolation model response (Fig. 10) split into its (a) numerator N(α) and denominator D(α) components and (b) their respective derivatives.

The even order propagation constants γ/k_0 of the first six modes at 20 GHz are listed in Table 7 together with Huang's results [53]. Huang used the singular integral equation method to determine the propagation constants. Fig. 13 shows all the even order modes versus frequency. Evanescent modes $\gamma/k_0 = \alpha/k_0$ are plotted in the opposite direction.

Table 7. Propagation constant γ/k_0 of the first six even order modes for the microstrip line (Fig. 9) at 20 GHz.

	Mode 1	Mode 2	Mode 3	Mode 4	Mode 5	Mode 6
Huang [53]	j2.7086	j1.1031	j0.72499	j0.59418	0.55274	0.77162 ± j0.15345
This Method	j2.7106	j1.1027	j0.72511	j0.59457	0.55192	0.75304 ± j0.14338

The number of characteristic equation evaluations to determine all the propagation constants versus frequency is shown in Fig. 14 evaluated in increments of 0.1 GHz. The complexity of the function increases as frequency increases and so the number of characteristic equation evaluations increase. From 16.4 GHz the number of divisions on the α-axis increases to two, and at 22.3 GHz and 23.0 GHz and from 23.2 GHz the number of divisions is three. Fig. 15 shows that between 3 and 15 evaluations are required per determination of an imaginary or a real root over the interval of interest. The calculation of roots via a previously published technique [56] required between 100 and 300 evaluations of the characteristic equation to determine the roots between adjacent poles. Note that the number of poles over the interval of interest is between 3 and 8, resulting in a typical reduction of a factor 100 in computational effort.

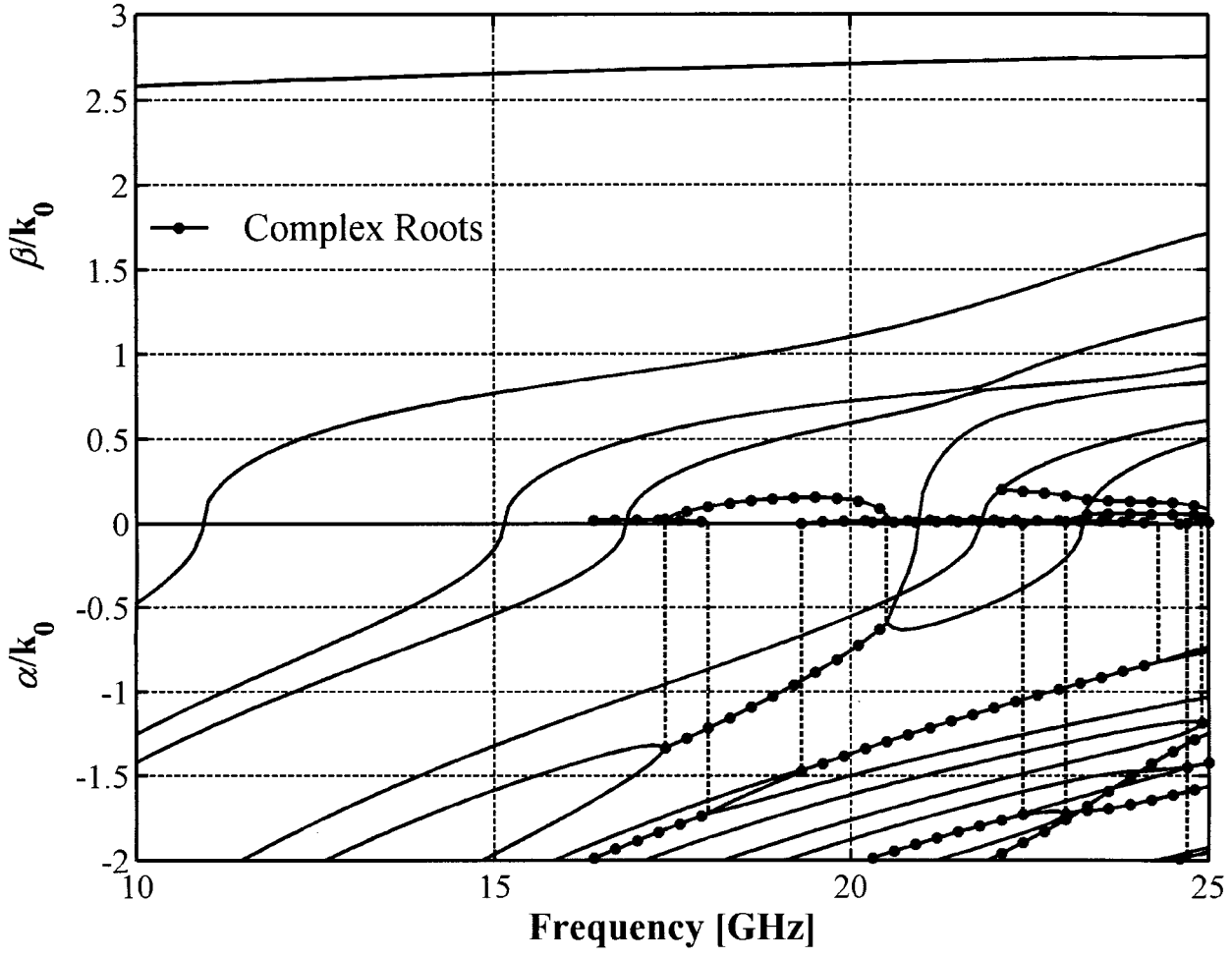

Fig. 13. Even order propagation constants $\gamma = \alpha + j\beta$ normalised with k_0 versus frequency for the shielded microstrip line structure (Fig. 9).

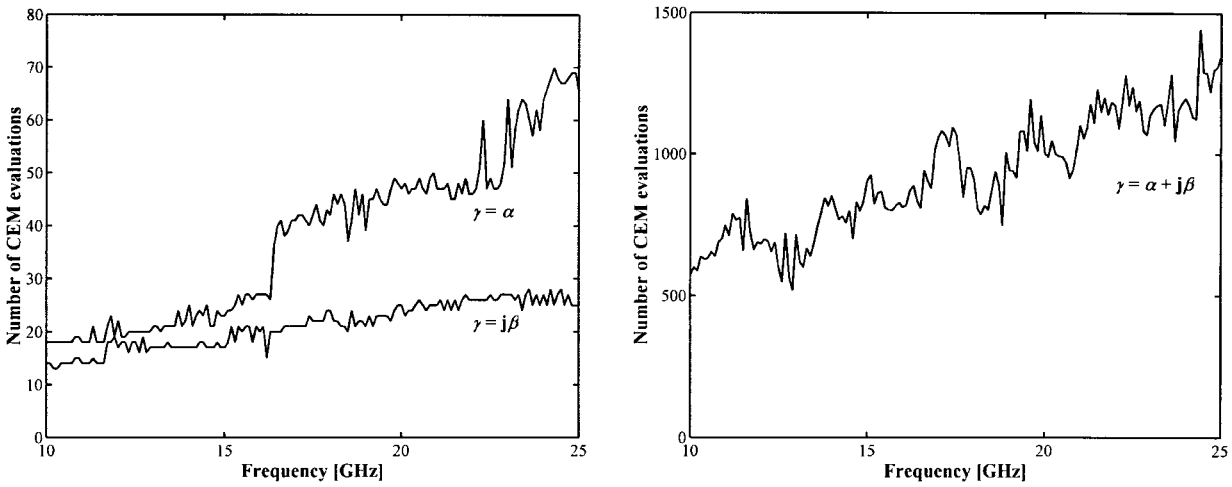

(a) (b)

Fig. 14. The number of characteristic equation evaluations versus frequency required by the adaptive sampling algorithm to establish a model for the shielded microstrip line structure with (a) $\gamma = j\beta$ and $\gamma = \alpha$, and (b) $\gamma = \alpha + j\beta$.

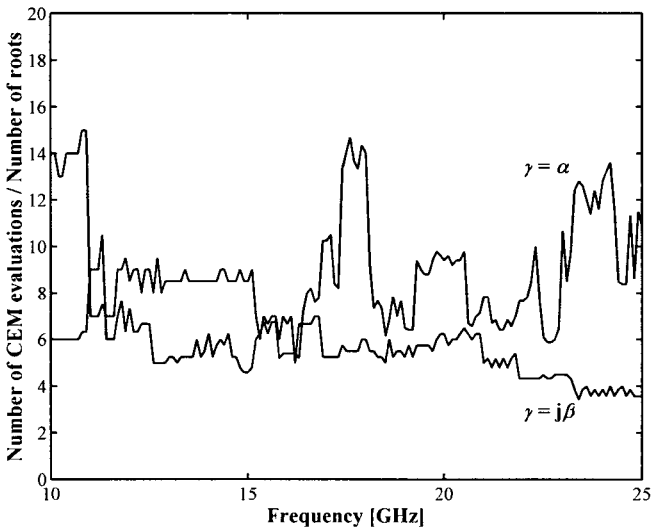

Fig. 15. The number of characteristic equation evaluations per number of roots found versus frequency for both $\gamma = j\beta$ and $\gamma = \alpha$ for the shielded microstrip line structure (Fig. 9).

4.2.2 Unilateral fin line

The guide wavelength λ is evaluated for the unilateral fin line with a centred slot as shown in Fig. 16. The wavelength inside the guide is $2\pi/\beta_0$, where β_0 is the dominant mode. Fig. 17 shows the guide wavelength λ normalised with the free space wavelength λ_0 versus frequency for different values of the slot width, w. Table 8 compares the computed results with those given in [65, Table 4.4], where spectral domain formulas and modal analysis were used.

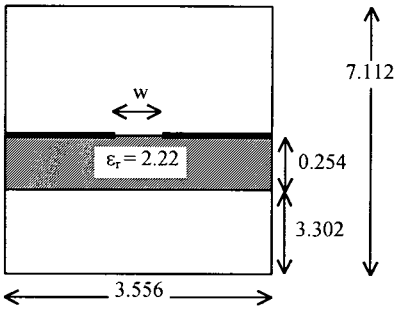

Fig. 16. Cross-section of the centred slot unilateral fin line. All dimensions are given in millimetres.

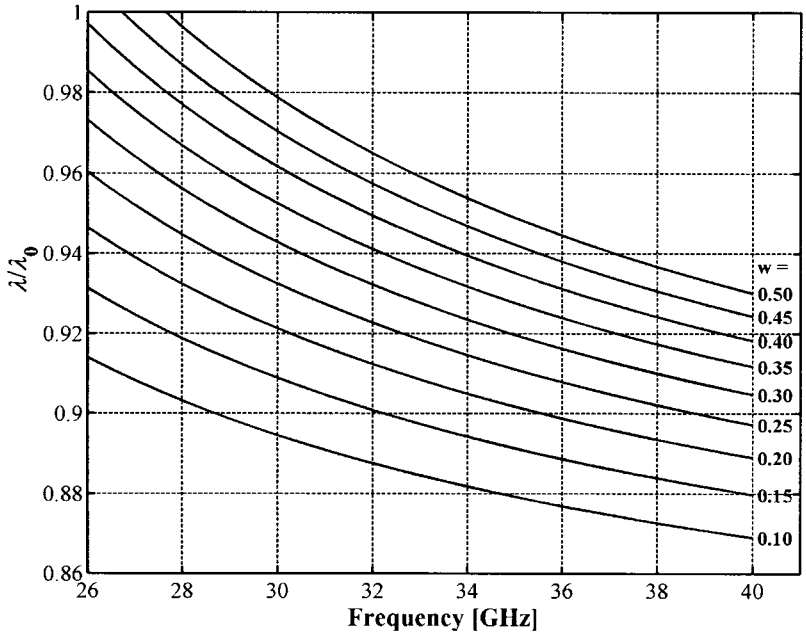

Fig. 17. Normalised guide wavelength λ/λ_0 versus frequency for the centred slot unilateral fin line structure (Fig. 16). The slot width w is given in millimetres.

Table 8. Comparison of the guide wavelength λ/λ_0 for the unilateral fin line structure (Fig. 16) with w = 0.5 mm.

Frequency [GHz]	λ/λ_0		
	Modal analysis [65]	Spectral domain [65]	This Method
26.0	1.1096	1.0200	1.0192
30.0	0.9791	0.9794	0.9789
35.0	0.9491	0.9494	0.9490
40.0	0.9302	0.9304	0.9301

4.3 Conclusions

The examples presented in this chapter illustrate the use of the adaptive sampling algorithm for the modelling of univariate problems. In the first example, the adaptive sampling algorithm was integrated into the ASM optimisation technique, which provided an automatic and efficient way to minimise the CEM frequency evaluations. An arbitrary number of frequency points required by the parameter extraction optimisation can be calculated from the surrogate model, which ensured the

non-failure of the parameter extraction step. The new technique worked well when applied to the design of a low-pass compact rectangular waveguide filter with capacitive step discontinuities.

In the second example, the adaptive sampling algorithm was applied to the two-dimensional Method-of-Lines technique for the calculation of transmission line characteristics of two- and three-layer shielded planar structures. An efficient selection of a minimum number of propagation constant support points defined an accurate rational function model for the characteristic equation to which a fast root finding algorithm was applied. The application of the method to the analyses of a shielded microstrip line structure and a unilateral fin line structure required typically between 3 and 15 evaluations of the characteristic function to determine an imaginary or a real zero.

CHAPTER 5: RESULTS – MULTIVARIATE ADAPTIVE SAMPLING

A number of two- and three-dimensional models were created for standard microwave circuits for verification of the adaptive sampling algorithms. To determine the accuracy of the models, they had to be evaluated on an independent evaluation data set, similar to the validation procedures applied to neural network models. In the following examples, the relative squared error E_m between the function and the model was calculated on rectangular equi-spaced grids with 30^2 grid points for the bivariate cases and a 20^3 grid points for the trivariate cases. In all cases, both the mean and the maximum errors in dB are shown for models of varying size. None of these models were reduced in size after a fit was obtained, in contrast to techniques where the order of the interpolant is guessed beforehand, and the interpolation function (calculated by a high number of CEM analyses) is systematically reduced afterwards. Section 5.1 illustrates results of the adaptive sampling algorithms, ASA1 and ASA2 [33]-[35], for the multivariate single output models, and section 5.2 shows the results of the adaptive sampling algorithm, ASA3, for the multivariate multiple output models all of which are applied to several passive microwave structures.

5.1 Single output models

5.1.1 Stripline characteristic impedance – 2 variables

A bivariate model $\Re(w/h, \varepsilon_r)$ was created with the adaptive sampling algorithm for the characteristic impedance $Z_0(w/h, \varepsilon_r)$ of a homogeneous symmetric stripline as shown in Fig. 18. The variables are: the strip width-to-height ratio w/h and the relative dielectric constant ε_r of the substrate. The strip conductor was assumed to be infinitesimally thin, thus $Z_0(w/h, \varepsilon_r)$ can be computed using the exact formula, which is derived using a conformal transformation [66]. Note that in practice, a CEM analysis will be used. The model is established for the parameters $w/h \in [0.05, 1]$ and $\varepsilon_r \in [1, 25]$, which define the interpolation space. At initialisation, the 9 chosen support points produce $\Re(w/h, \varepsilon_r)$ with the maximum error equal to −16.4 dB. Table 9 shows the convergence of the models using ASA1 and ASA2 as the number of support points increase. With equivalent accuracies (−57 dB) the model constructed by ASA2 required 7 fewer support points than ASA1. The response of the interpolation model $\Re(w/h, \varepsilon_r)$ with 36 support points constructed with ASA1 and its relative squared error $E_m(w/h, \varepsilon_r)$ are shown in Fig. 19. Fig. 20 represents the response of the interpolation model $\Re(w/h, \varepsilon_r)$ with 29 support points constructed with ASA2 and its relative squared error $E_m(w/h, \varepsilon_r)$, which is less than −56 dB in the interpolation space.

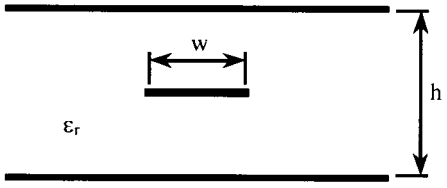

Fig. 18. Cross sectional view of the stripline.

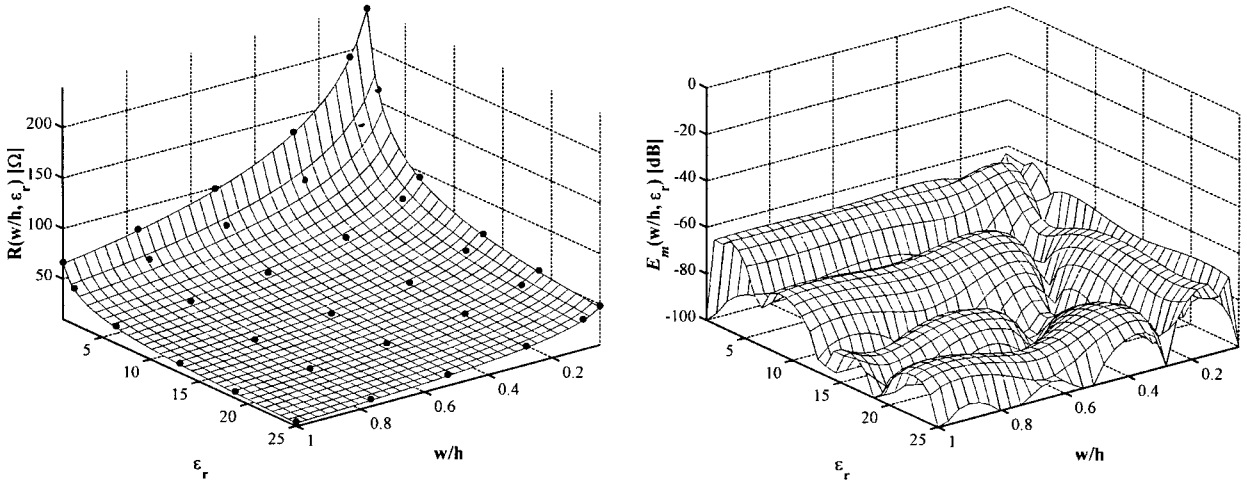

(a) (b)

Fig. 19. ASA1: Stripline example. (a) Response $\Re(w/h, \varepsilon_r)$ and (b) error $E_m(w/h, \varepsilon_r)$ with 36 support points.

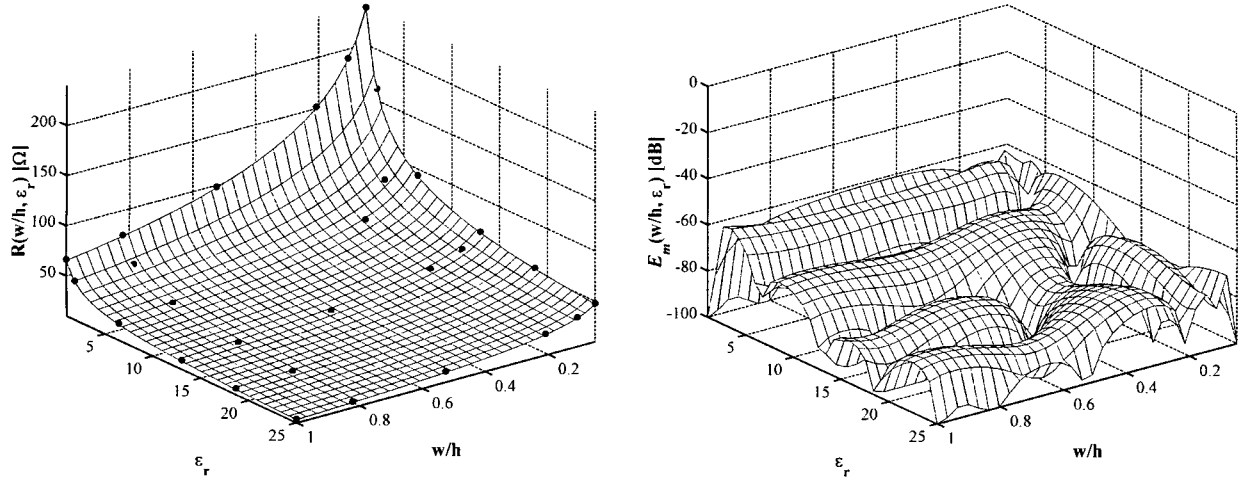

(a) (b)

Fig. 20. ASA2: Stripline example. (a) Response $\Re(w/h, \varepsilon_r)$ and (b) error $E_m(w/h, \varepsilon_r)$ with 29 support points.

Table 9. Convergence of $\Re(w/h, \varepsilon_r)$ determined by ASA1 and ASA2 for the stripline example.

ASA1			ASA2		
Number of support points	$E_m(w/h, \varepsilon_r)$ [dB]		Number of support points	$E_m(w/h, \varepsilon_r)$ [dB]	
	Mean	Max		Mean	Max
9	−29.3	−16.4	9	−29.3	−16.4
16	−40.4	−25.9	14	−33.0	−18.5
24	−42.4	−30.0	21	−42.4	−29.1
36	−74.5	−58.8	29	−72.3	−56.9

5.1.2 Capacitive step in rectangular waveguide – 2 variables

Bivariate models $\Re_{11}(f, h)$ and $\Re_{21}(f, h)$, and $\Re_{11}(f, l)$ and $\Re_{21}(f, l)$, were created for the reflection and transmission coefficients, i.e. $S_{11}(f, h)$ and $S_{21}(f, h)$, and $S_{11}(f, l)$ and $S_{21}(f, l)$, of a capacitive step in a rectangular waveguide as illustrated in Fig. 21. The variables are: frequency f and gap height h; and frequency f and gap length l. The models were constructed for a standard WR90 rectangular waveguide. The capacitive step was analysed using the mode matching method combined with the generalised scattering matrix [47]. The models $\Re_{11}(f, h)$ and $\Re_{21}(f, h)$ are established with $f \in [7\,\text{GHz}, 13\,\text{GHz}]$, $h \in [2\,\text{mm}, 8\,\text{mm}]$ and $l = 2\,\text{mm}$. The convergence of the models using ASA1 and ASA2 as the number of support points increases is tabulated in Table 10 and Table 11. The responses of the interpolation models $\Re_{11}(f, h)$ and $\Re_{21}(f, h)$ with 44 support points each determined with ASA2 and their relative squared errors are shown in Fig. 22 and Fig. 23 respectively.

Table 10. Convergence of $\Re_{11}(f, h)$ determined by ASA1 and ASA2 for the capacitive step example.

ASA1			ASA2		
Number of support points	$E_{11}(f, h)$ [dB]		Number of support points	$E_{11}(f, h)$ [dB]	
	Mean	Max		Mean	Max
12	−34.4	−20.3	15	−52.5	−35.4
16	−54.5	−45.7	20	−61.4	−44.9
20	−57.5	−45.0	22	−62.5	−48.2
30	−68.2	−50.5	37	−76.2	−51.1
42	−81.0	−70.1	44	−93.2	−82.3

Table 11. Convergence of $\Re_{21}(f, h)$ determined by ASA1 and ASA2 for the capacitive step example.

ASA1			ASA2		
Number of support points	$E_{21}(f, h)$ [dB]		Number of support points	$E_{21}(f, h)$ [dB]	
	Mean	Max		Mean	Max
12	−51.3	−38.0	13	−52.3	−44.8
15	−52.3	−38.0	18	−61.8	−51.9
25	−65.3	−53.6	22	−64.6	−28.4
35	−82.2	−61.2	37	−91.5	−71.3
42	−90.1	−78.5	44	−94.1	−80.7

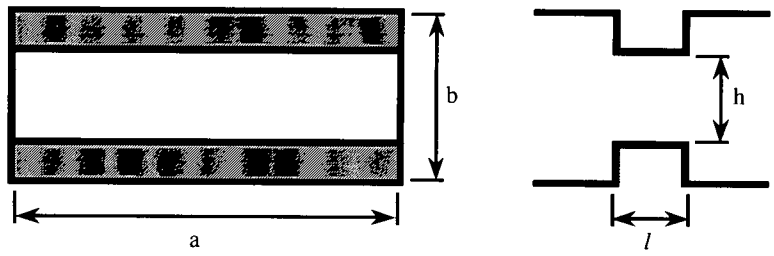

Fig. 21. Cross sectional view and side view of the capacitive step.

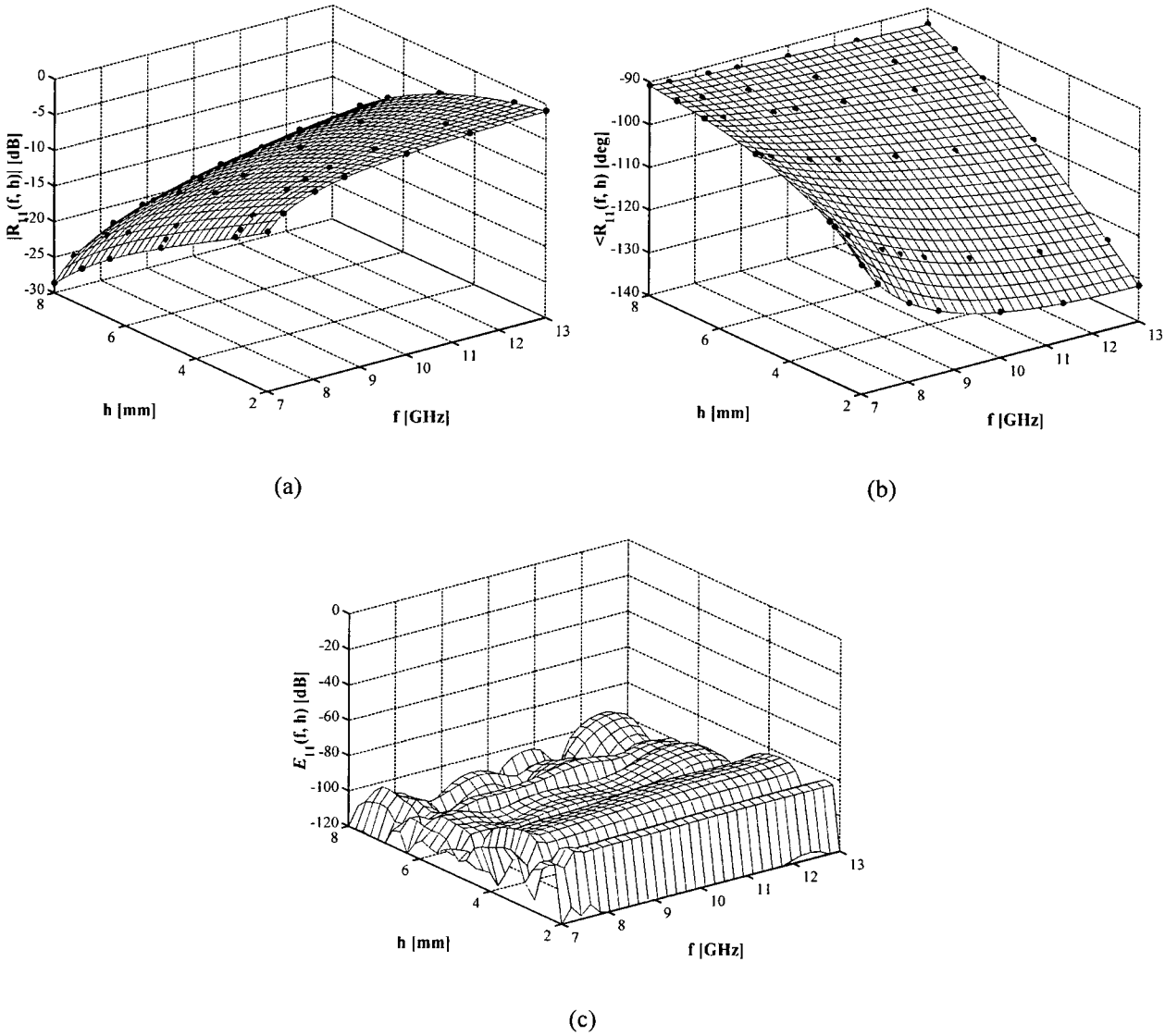

Fig. 22. ASA2: Capacitive step example. Magnitude (a) and phase (b) responses of $\Re_{11}(f, h)$ with 44 support points and its error $E_{11}(f, h)$ (c).

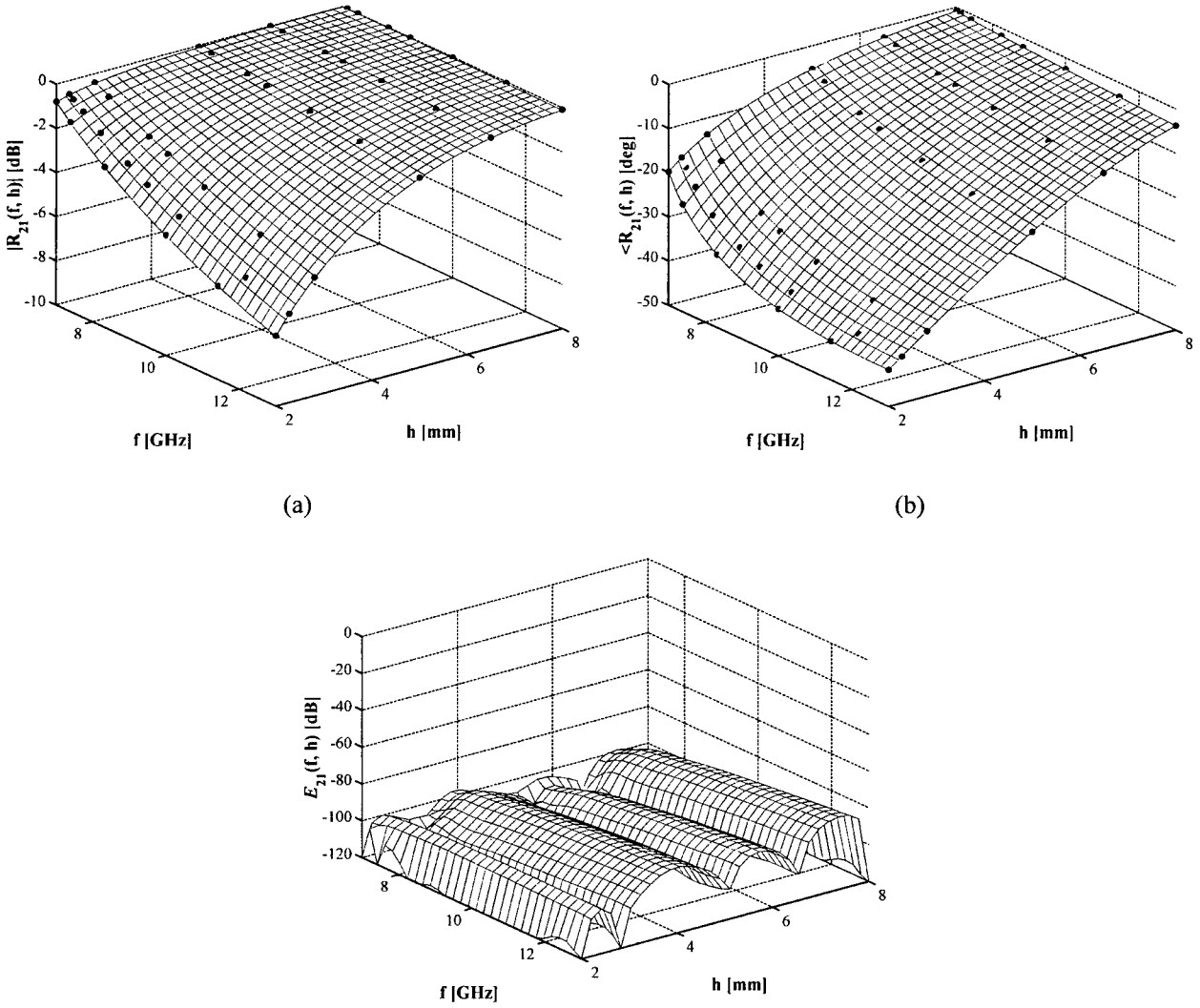

Fig. 23. ASA2: Capacitive step example. Magnitude (a) and phase (b) responses of $\Re_{21}(f, h)$ with 44 support points and its error $E_{21}(f, h)$ (c).

The models $\Re_{11}(f, l)$ and $\Re_{21}(f, l)$ are established with $f \in [7\text{ GHz}, 13\text{ GHz}]$, $l \in [0.5\text{ mm}, 5\text{ mm}]$ and $h = 5\text{ mm}$. Table 12 shows the convergence of the models using ASA2 as the number of support points increases. The responses of the models $\Re_{11}(f, l)$ and $\Re_{21}(f, l)$ with 45 and 42 support points and their relative squared errors are shown in Fig. 24 and Fig. 25 respectively. With equivalent number of support points the errors of the models determined by ASA2 tend to be less by up to 10 dB compared to those determined by ASA1.

Table 12. Convergence of $\Re_{11}(f, l)$ and $\Re_{21}(f, l)$ determined by ASA2 for the capacitive step example.

$\Re_{11}(f, l)$			$\Re_{21}(f, l)$		
Number of support points	$E_{11}(f, l)$ [dB]		Number of support points	$E_{21}(f, l)$ [dB]	
	Mean	Max		Mean	Max
12	−42.3	−22.1	12	−54.8	−38.0
17	−57.1	−40.2	16	−56.7	−36.2
21	−61.1	−50.7	19	−65.6	−51.8
45	−82.5	−63.8	42	−89.3	−71.1

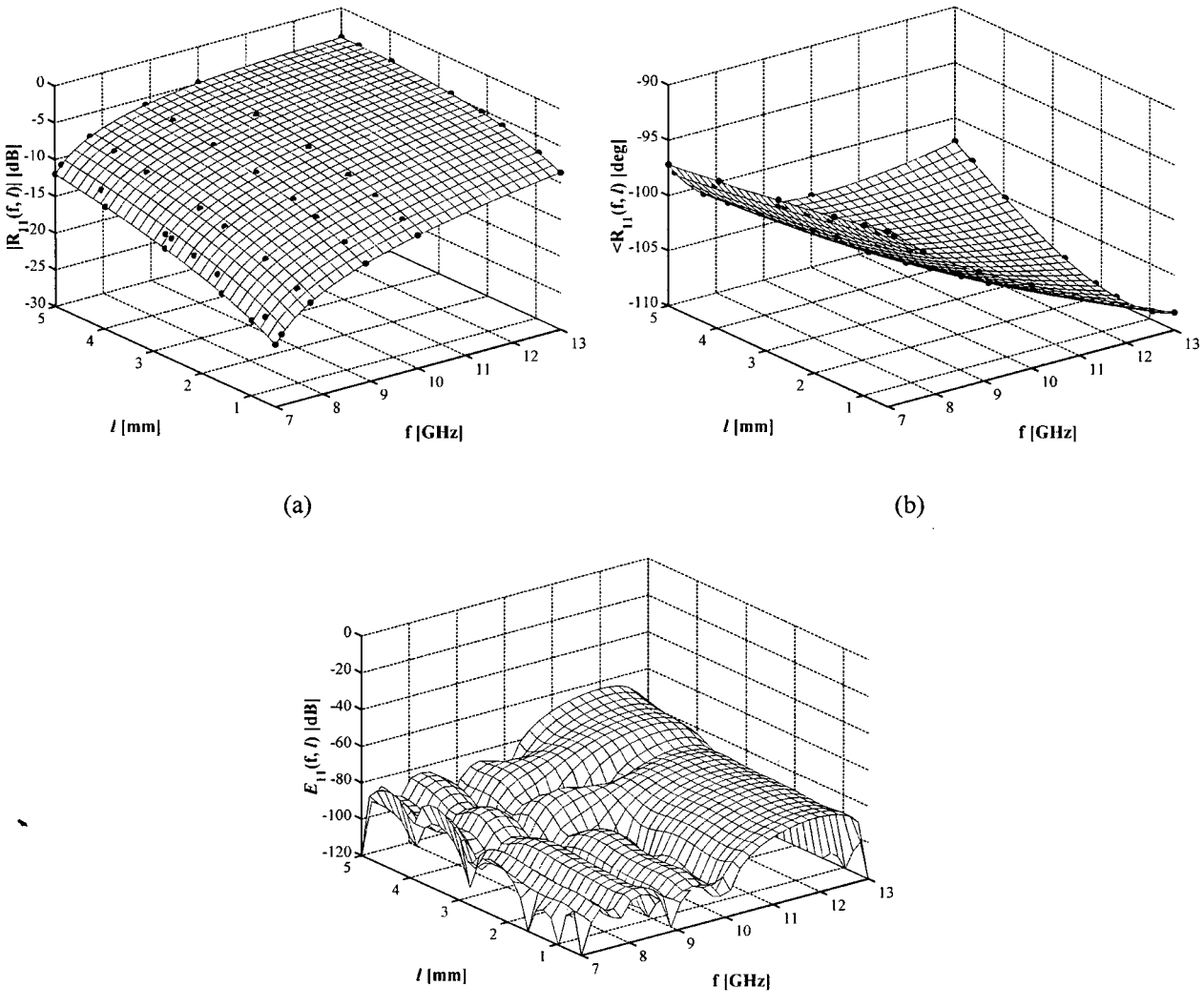

Fig. 24. ASA2: Capacitive step example. Magnitude (a) and phase (b) responses of $\Re_{11}(f, l)$ with 45 support points and its error $E_{11}(f, l)$ (c).

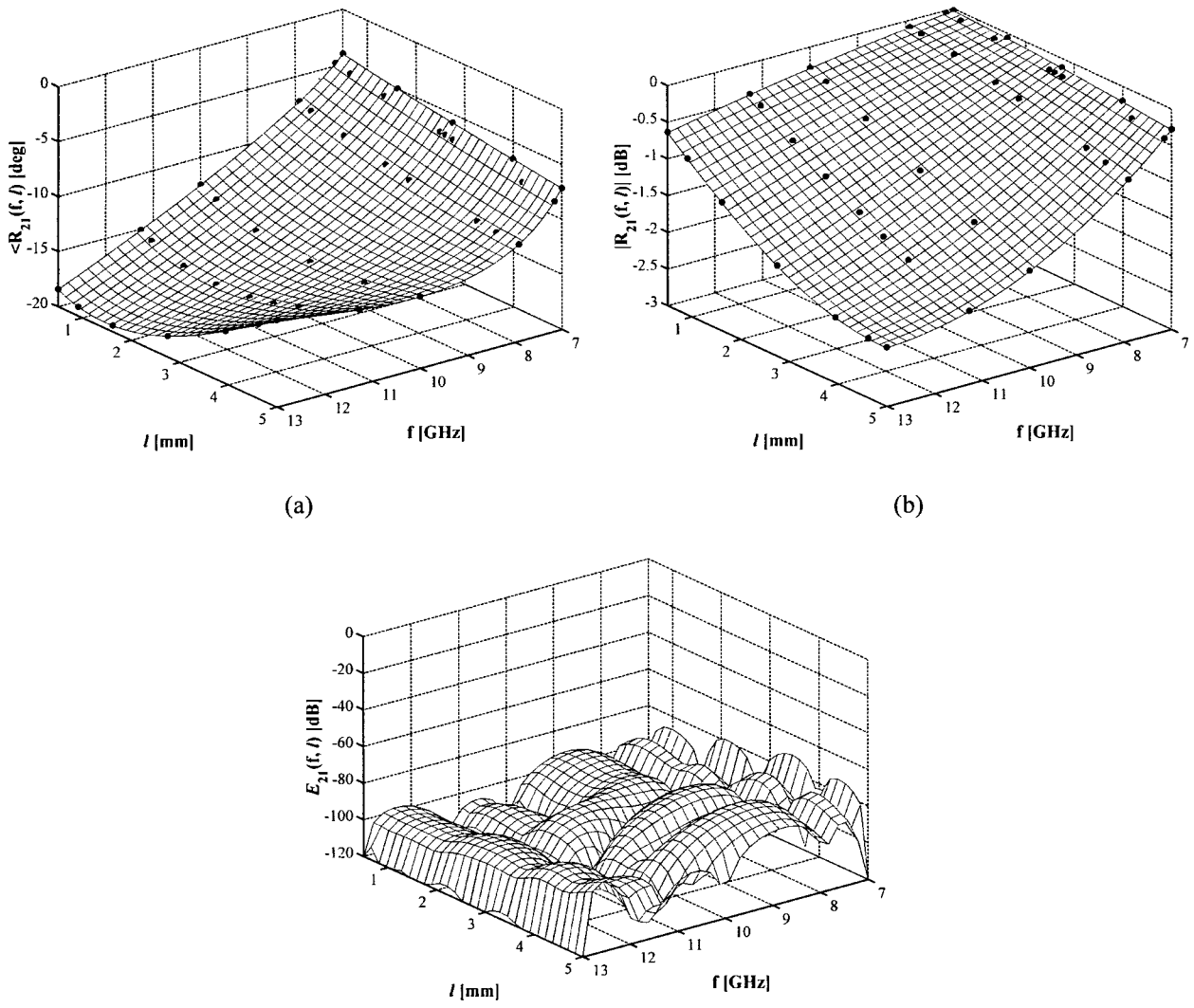

Fig. 25. ASA2: Capacitive step example. Magnitude (a) and phase (b) responses of $\Re_{21}(f, l)$ with 42 support points and its error $E_{21}(f, l)$ (c).

5.1.3 Inductive posts in rectangular waveguide – 2 variables

Bivariate models $\Re_{11}(f, w)$ and $\Re_{21}(f, w)$ were created for the reflection and transmission coefficients, i.e. $S_{11}(f, w)$ and $S_{21}(f, w)$, of two perfectly conducting round posts centred in the E-plane of a rectangular waveguide as shown in Fig. 26. The variables are: frequency f and post-spacing w. The diameter of the posts d was set to 2 mm and the model was constructed for a standard WR90 rectangular waveguide with $f \in [7\,\text{GHz}, 13\,\text{GHz}]$ and $w \in [4\,\text{mm}, 18\,\text{mm}]$. A moment method technique is used to analyse this structure [67]. Table 13 and Table 14 exemplify the convergence of the models $\Re_{11}(f, w)$ and $\Re_{21}(f, w)$ using ASA1 and ASA2 as the number of support points increase. The responses of the interpolation models $\Re_{11}(f, w)$ and $\Re_{21}(f, w)$ with 53 and 57 support points respectively established with ASA2 and their relative squared errors are shown in Fig. 27 and Fig. 28.

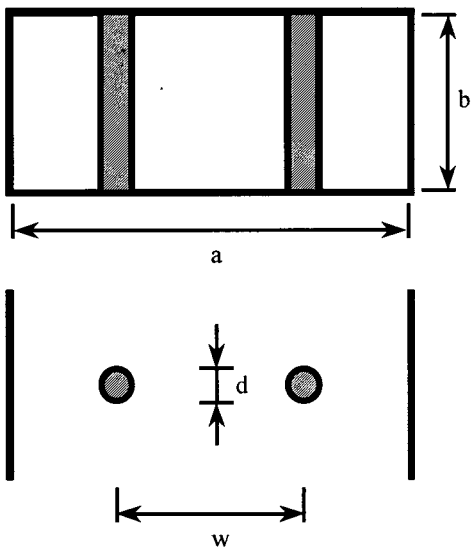

Fig. 26. Cross sectional view and top view of the inductive posts.

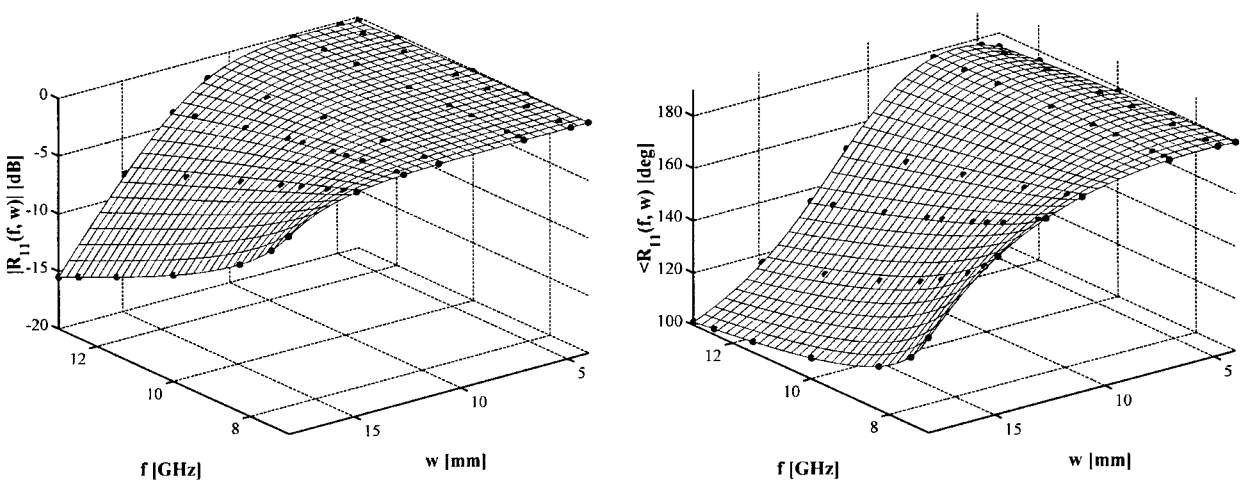

(a) (b)

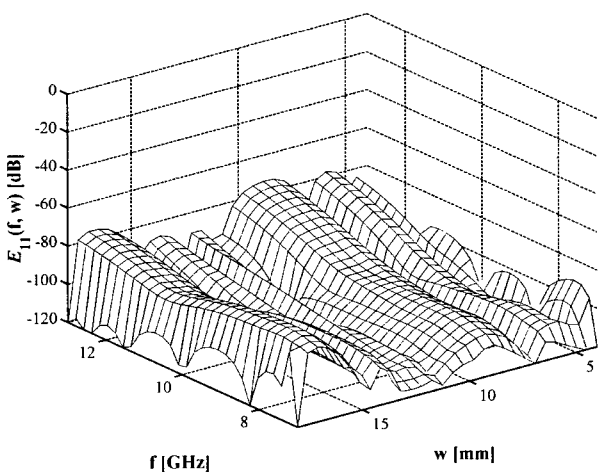

(c)

Fig. 27. ASA2: Inductive post example. Magnitude (a) and phase (b) responses of $\Re_{11}(f, w)$ with 53 support points and its error $E_{11}(f, w)$ (c).

Table 13. Convergence of $\Re_{11}(f, w)$ determined by ASA1 and ASA2 for the inductive posts example.

ASA1			ASA2		
Number of support points	$E_{11}(f, w)$ [dB]		Number of support points	$E_{11}(f, w)$ [dB]	
	Mean	Max		Mean	Max
18	−32.4	−16.8	18	−38.1	−23.7
36	−39.8	−13.8	28	−67.2	−49.2
48	−88.4	−73.8	53	−91.5	−73.7

Table 14. Convergence of $\Re_{21}(f, w)$ determined by ASA1 and ASA2 for the inductive posts example.

ASA1			ASA2		
Number of support points	$E_{21}(f, w)$ [dB]		Number of support points	$E_{21}(f, w)$ [dB]	
	Mean	Max		Mean	Max
18	−38.1	−25.1	23	−59.1	−41.6
36	−39.6	−9.2	30	−52.1	−27.4
48	−89.8	−68.6	51	−76.8	−51.3
56	−90.4	−64.9	57	−87.9	−72.5

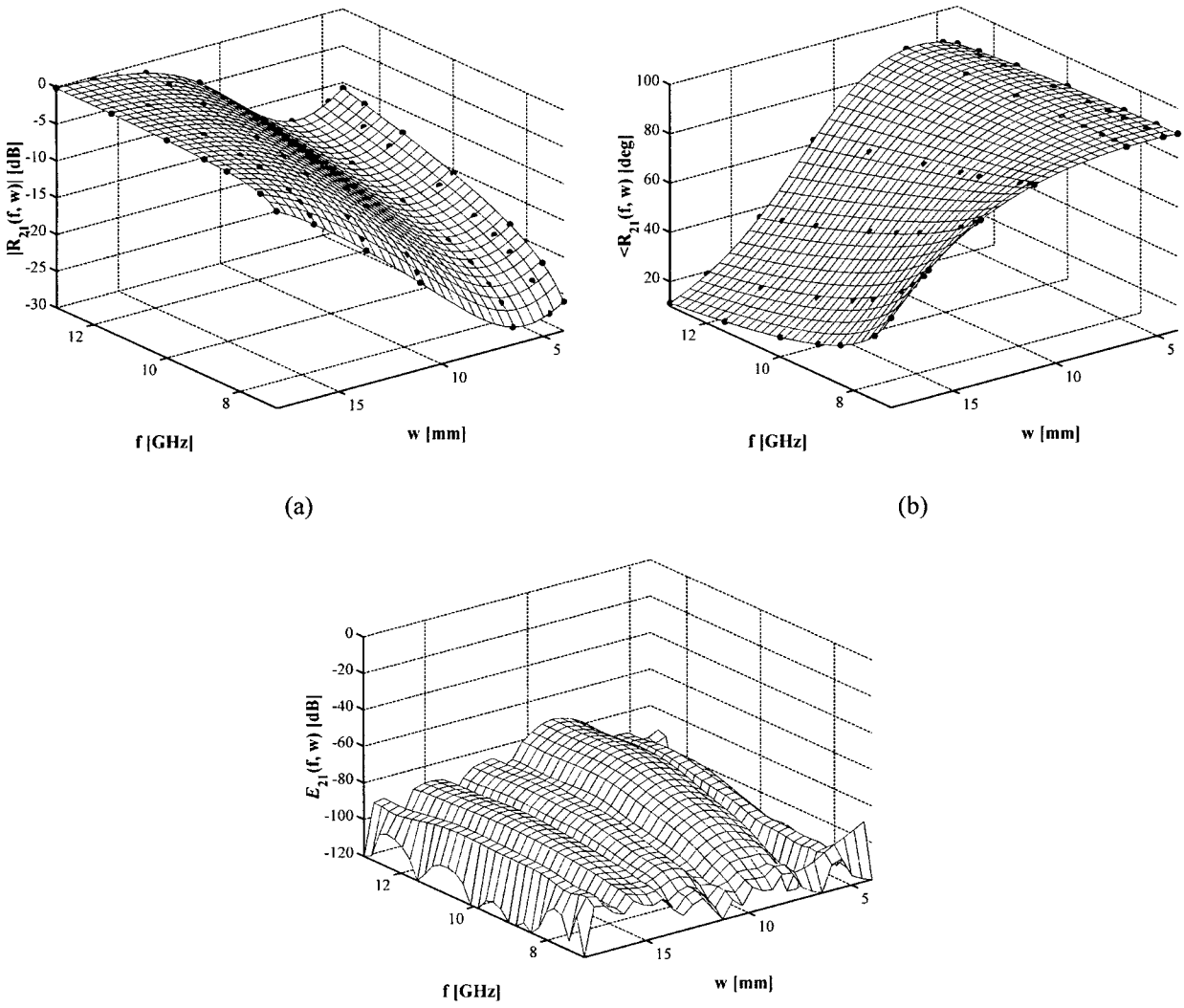

Fig. 28. ASA2: Inductive post example. Magnitude (a) and phase (b) responses of $\Re_{21}(f, w)$ with 57 support points and its error $E_{21}(f, w)$ (c).

5.1.4 Capacitive step in rectangular waveguide – 3 variables

A trivariate model $\Re_{11}(f, h, l)$ was constructed for the reflection coefficient, i.e. $S_{11}(f, h, l)$ of a capacitive step in a rectangular waveguide as shown in Fig. 21. The variables are: frequency f, gap height h and step length l. The model was created for a standard WR90 rectangular waveguide. The capacitive step is analysed using the mode matching method [47]. Two sets of models were established with different interpolation spaces, i.e. a) $f \in [8\text{ GHz}, 12\text{ GHz}]$, $h \in [3\text{ mm}, 7\text{ mm}]$ and $l \in [1\text{ mm}, 4\text{ mm}]$; and b) $f \in [7\text{ GHz}, 13\text{ GHz}]$, $h \in [2\text{ mm}, 8\text{ mm}]$ and $l \in [0.5\text{ mm}, 5\text{ mm}]$. Table 15 and Table 16 show the results using ASA1 and ASA2 respectively. For the smaller interpolation space the models constructed by ASA1 and ASA2 attain an error smaller than –95 dB with approximately 920 support points. ASA2 has a faster convergence than ASA1. For the larger interpolation space ASA1 failed to produce a model with good accuracy, due to the non-optimal placement of the support points, while ASA2 achieved an error of smaller than –58 dB with 2142 support points.

Table 15. Convergence of $\Re_{11}(f, h, l)$ determined by ASA1 for the capacitive step example.

$f \in [8\text{ GHz}, 12\text{ GHz}]$, $h \in [3\text{ mm}, 7\text{ mm}]$, $l \in [1\text{ mm}, 4\text{ mm}]$			$f \in [7\text{ GHz}, 13\text{ GHz}]$, $h \in [2\text{ mm}, 8\text{ mm}]$, $l \in [0.5\text{ mm}, 5\text{ mm}]$		
Number of support points	$E_{11}(f, h, l)$ [dB]		Number of support points	$E_{11}(f, h, l)$ [dB]	
	Mean	Max		Mean	Max
64	–65.1	–49.5	150	–56.6	–31.1
180	–82.2	–55.5	294	–62.0	–30.1
294	–85.3	–59.5	576	–59.3	–15.1
512	–100.8	–63.1	1300	–81.0	–32.1
832	–108.2	–76.6	1716	–83.2	–35.0
936	–109.3	–96.8	2730	–70.0	–26.7

Table 16. Convergence of $\Re_{11}(f, h, l)$ determined by ASA2 for the capacitive step example.

$f \in [8\text{ GHz}, 12\text{ GHz}]$, $h \in [3\text{ mm}, 7\text{ mm}]$, $l \in [1\text{ mm}, 4\text{ mm}]$			$f \in [7\text{ GHz}, 13\text{ GHz}]$, $h \in [2\text{ mm}, 8\text{ mm}]$, $l \in [0.5\text{ mm}, 5\text{ mm}]$		
Number of support points	$E_{11}(f, h, l)$ [dB]		Number of support points	$E_{11}(f, h, l)$ [dB]	
	Mean	Max		Mean	Max
115	–70.7	–21.9	343	–55.5	–15.3
164	–75.5	–46.7	593	–67.0	–31.4
300	–86.6	–57.8	737	–76.5	–40.0
379	–89.9	–75.8	871	–79.5	–47.0
496	–107.3	–86.0	1375	–91.7	–47.7
645	–108.3	–94.4	1758	–96.1	–54.7
917	–109.1	–97.5	2142	–97.2	–58.1

5.1.5 Iris in rectangular waveguide – 3 variables

A trivariate model $\Re_{21}(f, a, b)$ was created for the transmission coefficient, i.e. $S_{21}(f, a, b)$ of an iris in a rectangular waveguide as illustrated in Fig. 29. The variables are: frequency f, gap width a and gap height b. The model was constructed for a standard WR90 rectangular waveguide with

$f \in [8\text{ GHz}, 12\text{ GHz}]$, $a \in [8\text{ mm}, 15\text{ mm}]$, $b \in [1\text{ mm}, 3\text{ mm}]$ and $l = 1$ mm. The iris is analysed using the mode matching method [47]. Table 17 and Table 18 show the results using ASA1 and ASA2. ASA1 failed to produce a model with good accuracy, due to the non-optimal placement of the support points, while ASA2 achieved an error of smaller than –52 dB with 736 support points.

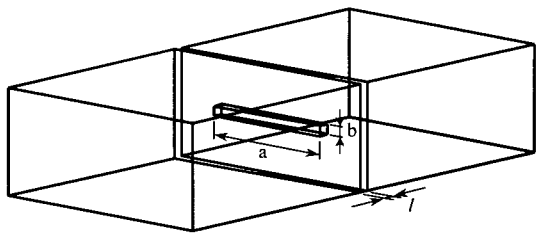

Fig. 29. Iris in rectangular waveguide.

Table 17. Convergence of $\Re_{21}(f, a, b)$ determined by ASA1 for the iris example.

Number of support points	$E_{21}(f, a, b)$ [dB]	
	Mean	Max
252	–37.9	–3.6
1120	–46.2	–7.4
1440	–44.3	–1.5

Table 18. Convergence of $\Re_{21}(f, a, b)$ determined by ASA2 for the iris example.

Number of support points	$E_{21}(f, a, b)$ [dB]	
	Mean	Max
168	–50.0	–18.0
247	–56.9	–19.5
328	–63.2	–31.1
560	–66.5	–33.1
736	–72.7	–52.6

5.2 Multiple output models

Bivariate, multiple output models were constructed for the same structures as given in section 5.1, where single output interpolation models were constructed for each of the scattering parameters. This was done in order to illustrate the efficiency of the multiple output models relative to that of the single output models.

5.2.1 Capacitive step in rectangular waveguide – 2 variables

A bivariate, multiple output model $\Re(f, h)$ was created for the reflection and transmission coefficients, i.e. $S_{11}(f, h)$ and $S_{21}(f, h)$, of a capacitive step in a rectangular waveguide as shown in Fig. 21 and the results are tabulated in Table 19. Table 20 shows the results for the model $\Re(f, l)$,

which models $S_{11}(f, l)$ and $S_{21}(f, l)$. The parameters for both models $\Re(f, h)$ and $\Re(f, l)$ are the same as those given in section 4.2.2. Comparison of these results with those of Table 10, Table 11 and Table 12, where separate models were constructed for the reflection and the transmission coefficients, shows that with equivalent model accuracies the total number of support points is halved.

Table 19. Convergence of $\Re(f, h)$ determined by ASA3 for the capacitive step example.

Number of support points	$E_{11}(f, h)$ [dB]		$E_{21}(f, h)$ [dB]	
	Mean	Max	Mean	Max
15	−52.5	−35.4	−54.8	−37.0
20	−61.3	−44.6	−66.1	−47.2
22	−62.5	−48.3	−65.0	−36.4
37	−76.3	−51.2	−89.9	−65.0
42	−96.4	−85.2	−98.5	−85.7

Table 20. Convergence of $\Re(f, l)$ determined by ASA3 for the capacitive step example.

Number of support points	$E_{11}(f, l)$ [dB]		$E_{21}(f, l)$ [dB]	
	Mean	Max	Mean	Max
12	−42.8	−22.1	−54.0	−36.6
18	−59.0	−47.9	−65.0	−55.2
22	−61.1	−51.2	−65.4	−55.2
46	−82.4	−63.8	−86.3	−69.0

5.2.2 Inductive post in rectangular waveguide – 2 variables

A bivariate, multiple output model $\Re(f, w)$ for an inductive post in a rectangular waveguide as shown in Fig. 26 was created for the reflection and transmission coefficients, i.e. $S_{11}(f, w)$ and $S_{21}(f, w)$. The results are shown in Table 21. The parameters for the models $\Re(f, w)$ are the same as those given in section 4.2.3. Comparison of these results with those of Table 13 and Table 14, where separate models were constructed for the reflection and the transmission coefficients, shows that with equivalent model accuracies the total number of support points is approximately halved.

Table 21. Convergence of $\Re(f, w)$ determined by ASA3 for the inductive post example.

Number of support points	$E_{11}(f, w)$ [dB]		$E_{21}(f, w)$ [dB]	
	Mean	Max	Mean	Max
23	−61.7	−43.4	−58.7	−41.2
29	−69.3	−54.5	−67.2	−51.6
45	−77.8	−59.6	−78.4	−67.2
56	−87.8	−64.1	−85.7	−70.1

5.2.3 Longitudinal slot in common broad wall of two rectangular waveguides – 3 variables

A multivariate, multiple output model $\Re(f, l, d)$ was created to characterise a longitudinal slot in the common broad wall of two rectangular waveguides as illustrated in Fig. 30. The scattering parameters that completely define such a discontinuity are $S_{11}(f, l, d)$, $S_{21}(f, l, d)$ and $S_{31}(f, l, d)$. The port numbers are shown in Fig. 30 with port 1 being the incident port. The variables are: frequency f, slot length l and slot distance from the waveguide sidewall d. The model was established for a standard WR90 rectangular waveguide with $f \in [8\,\text{GHz}, 12\,\text{GHz}]$, $l \in [3.5\,\text{mm}, 10\,\text{mm}]$, $d \in [1\,\text{mm}, 11\,\text{mm}]$, slot height $t = 2.54\text{mm}$ and slot width $w = 0.5\,\text{mm}$. The structure is analysed using the method of moments [68]. Table 22 shows the accuracy of the model as the number of support points increase. An error of smaller than –58dB was achieved for all of the scattering parameters with only 577 support points. Fig. 31 shows the maximum relative errors $E_{i1}(f, l) = \max_{d \in [1,11]} E_{i1}(f, l, d)$ for all of the modelled scattering parameters of the multiple output interpolation model with 577 support points.

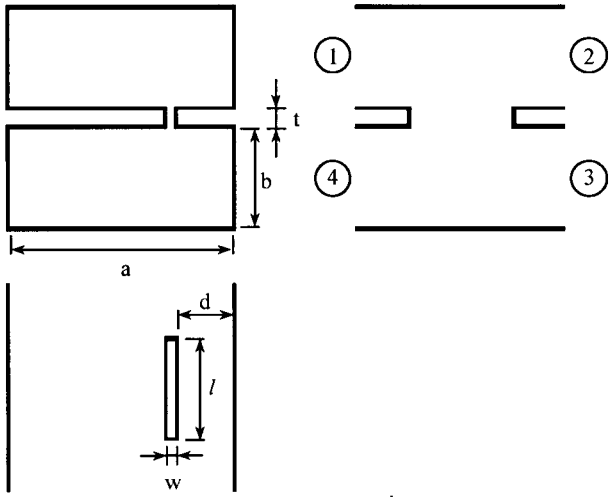

Fig. 30. Cross sectional view, top view and side view of the longitudinal slot in the common broad wall of two rectangular waveguides.

Table 22. Convergence of $\Re(f, l, d)$ determined by ASA3 for the capacitive step example.

Number of support points	$E_{11}(f, l, d)$ [dB]		$E_{21}(f, l, d)$ [dB]		$E_{31}(f, l, d)$ [dB]	
	Mean	Max	Mean	Max	Mean	Max
301	–58.2	–14.2	–62.8	–39.4	–60.3	–17.7
403	–66.0	–35.9	–73.5	–51.8	–70.0	–38.8
536	–71.3	–47.8	–70.6	–48.8	–74.0	–48.0
577	–73.6	–57.7	–78.5	–63.3	–76.8	–59.8

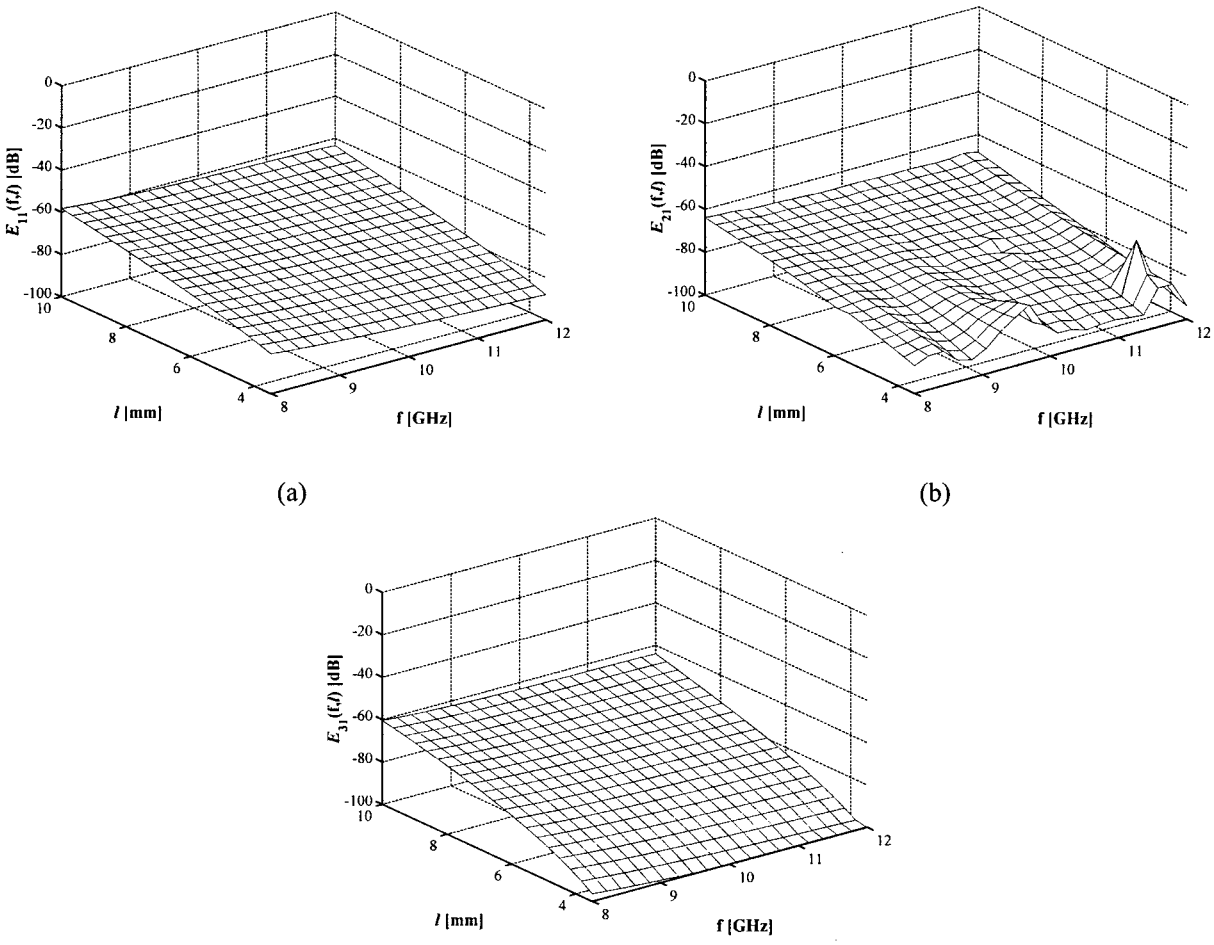

Fig. 31. ASA3: Longitudinal slot example. Maximum relative error $E_{i1}(f, l) = \max_{d \in [1, 11]} E_{i1}(f, l, d)$ of $\Re(f, l, d)$ with 577 support points for the scattering parameter $S_{i1}(f, l, d)$. (a) $i = 1$, (b) $i = 2$, (c) $i = 3$.

5.3 Conclusions

In this chapter the adaptive sampling algorithm applied to multivariate, multiple output models was evaluated on a number of passive microwave circuits. Errors of smaller than 0.25 % in the interpolation space were achieved in all cases. This model accuracy, which depends on the number of support points, is more than adequate for the purposes of designing most microwave circuits. It is shown that the adaptive sampling algorithm, which places support points on a non-rectangular grid, converges faster than an algorithm that places support points on a rectangular grid. The adaptive sampling algorithm for the multiple output models requires approximately the same number of support points as by the adaptive sampling algorithm for the single output model.

In summary, the results show clearly that the adaptive sampling algorithm can be used to good effect in the modelling of microwave circuits.

CHAPTER 6: EXTENSIONS AND CONCLUSIONS

6.1 Extensions

Different rational interpolants can be constructed from a single set of support points with varying degrees of accuracy. The method presented in this dissertation is general in the sense that it was not tuned for specific problems. However, different numberings of the support points may produce better results especially if knowledge of the function being modelled can be incorporated into the modelling algorithm.

In this dissertation the support points are essentially selected for a number of single variable functions in a multivariable interpolation space, which is computationally efficient. However, a multivariate interpolation technique that has the ability to choose support points totally arbitrarily in the interpolation space may be more optimal. This requires a different type of interpolant from the one used in this dissertation. Such a method will be computationally less efficient, because the whole interpolation space needs to be searched for the selection of new support points.

The modelling of highly non-linear functions can cause the order of the interpolant to become large, which can cause the interpolant to become numerically unstable. In this case the interpolation space needs to be subdivided into smaller interpolation spaces. The univariate adaptive sampling algorithm automatically divides the interpolation interval into smaller intervals when the order of the interpolant becomes too large. In the multivariate case subdivision is only applied to the set of univariate interpolants from which the multivariate interpolant is established. A possible extension would be to automatically divide the whole multivariate interpolation space into smaller interpolation spaces when required.

The most important extension to the multivariate adaptive sampling algorithm presented here would be the development of a method that can handle CEM analyses with significant numerical errors. An interpolant will create a curve that passes through all of the support points. Therefore, numerical errors will be incorporated into the model, which implies a high order interpolant. For these cases an approximant to the function being modelled would need to be found so that it be approximated rather than replicated.

6.2 Conclusions

In this dissertation an accurate and robust adaptive sampling algorithm was developed that used multivariate rational interpolants based on Thiele-type branched continued fractions to map a multi-

dimensional complex numbered input vector to a multi-dimensional complex numbered output vector. The multivariate interpolant was established from a combination of a set of univariate interpolants. Starting with low order interpolants, the technique systematically increased the order by optimally choosing new support points in the areas of highest error, until an accurate mathematical model with the desired accuracy was achieved.

The standard branched continued fraction interpolation technique, which required a fully filled rectangular grid of support points, was adapted to allow sampling on a more optimal non-rectangular grid. The coefficients of the rational interpolant and the evaluation of the function values were determined in a recursive manner, which made the sampling algorithm fast and efficient. An error estimate was obtained as a natural consequence of the recursion.

The adaptive sampling algorithm automatically and efficiently selected and minimised the sample points, which allowed model development without any *a priori* knowledge of the microwave structure under study.

The method was evaluated on a number of passive microwave circuits. In all cases an error of less than 0.25 % in the interpolation space was achieved. It was shown that the adaptive sampling algorithm, which placed support points on a non-rectangular grid, was superior to an algorithm that placed support points on a rectangular grid. Comparison of the adaptive sampling algorithms for single and multiple output models showed that the number of support points determined for a multiple output model was equivalent to that determined for a single output model.

In conclusion, the method presented here offers a viable technique for the creation of multi-input multi-output surrogate mathematical models for physical problems. Although the method was applied only to the CEM field, it is widely applicable and is in no way restricted to the specific examples shown here.

REFERENCES

[1] A. J. Booker, J. E. Dennis, Jr., P. D. Frank, D. B. Serafini, V. Torczon and M. W. Trosset, "A rigorous framework for optimization of expensive functions by surrogates," *Structural Optimization*, vol. 17, pp. 1-13, 1999.

[2] E. K. Miller, "Solving bigger problems – by decreasing the operation count and increasing the computation bandwidth," *Proc. IEEE*, vol. 79, no. 10, pp. 1493-1504, Oct. 1990.

[3] V. Rizzoli, A. Costanzo, C. Cecchetti and D. Masotti, "Computer-aided optimization of broadband nonlinear microwave integrated circuits with the aid of electromagnetically generated look-up tables," *Microwave Opt. Technol. Lett.*, vol. 15, no. 4, pp. 189-196, Jul. 1997.

[4] P. B. L. Meijer, "Fast and smooth highly nonlinear multidimensional table models for device modeling," *IEEE Trans. Circuits Syst.*, vol. 37, no. 3, pp. 335-346, Mar. 1990.

[5] P. Burrascano, S. Fiori and M. Mongiardo, "A review of artificial neural networks applications in microwave computer-aided design," *Int. J. RF and microwave CAE*, vol. 9, no. 3, pp. 158-174, May 1999.

[6] A. H. Zaabab, Q-J. Zhang and M. Nakhla, "A neural network modeling approach to circuit optimization and statistical design," *IEEE Trans. Microwave Theory Tech.*, vol. 43, no. 6, pp. 1349-1358, Jun. 1995.

[7] J. W. Bandler, R. M. Biernacki, S. H. Chen, J. Song, S. Ye and Q. J. Zhang, "Gradient quadratic approximation scheme for yield-driven design," *IEEE Int. Microwave Symp. Dig.*, Boston, MS, pp. 1197-1200, Jun. 1991.

[8] J-F. Liang and K. A. Zaki, "CAD of microwave junctions by polynomial curve fitting," *IEEE Int. Microwave Symp. Dig.*, Atlanta, FL, pp. 451-454, Jun. 1993.

[9] J. Carroll and K. Chang, "Statistical computer-aided design for microwave circuits," *IEEE Trans. Microwave Theory Tech.*, vol. 44, no. 1, pp. 24-32, Jan. 1996.

[10] Q-J. Zhang, F. Wang and M. Nakhla, "Optimization of high-speed VLSI interconnects: a review (invited article)," *Int. J. of Microwave and Millimeter-Wave CAE*, vol. 7, no. 1, pp. 83-107, Jan. 1997.

[11] E. G. Kogbetliantz, "Generation of elementary functions," *Mathematical methods for digital computers*, A. Ralston and H. S. Wilf (eds.), vol. 1, New York: John Wiley & Sons, 1960.

[12] E. W. Cheney and T. H. Southard, "A survey of methods for rational approximation, with particular reference to a new method based on a formula of Darboux", *SIAM Rev.*, vol. 5, no. 3, pp. 219-231, Jul. 1963.

[13] A. A. M. Cuyt, "A review of multivariate Padé approximation theory," *J. Comp. Appl. Math.*, vol. 12, pp. 221-232, 1985.

[14] A. Cuyt and L. Wuytack, *Nonlinear methods in numerical analysis*, North-Holland mathematics studies: 136, Studies in computational mathematics: 1, Amsterdam: Elsevier science publishers, 1987.

[15] P. R. Graves-Morris and T. R. Hopkins, "Reliable rational interpolation", *Numer. Math.*, vol. 36, pp. 111-128, 1981.

[16] A. A. M. Cuyt and B. M. Verdonk, "Multivariate rational interpolation," *Computing*, vol. 34, pp. 41-61, 1985.

[17] A. Cuyt, "A recursive computational scheme for multivariate rational interpolants," *SIAM J. Numer. Anal.*, vol. 24, no. 1, pp. 228-239, Feb. 1987.

[18] S. F. Peik, R. R. Mansour and Y. L. Chow, "Multidimensional Cauchy method and adaptive sampling for an accurate microwave circuit modeling," *IEEE Trans. Microwave Theory Tech.*, vol. 46, no. 12, pp. 2364-2371, Dec. 1998.

[19] J. Stoer and R. Bulirsch, *Introduction to numerical analysis*, Berlin: Springer-Verlag, 1980.

[20] J. Ureel, N. Faché, D. de Zutter and P. Lagasse, "Adaptive frequency sampling of scattering parameters obtained by electromagnetic simulation," *IEEE AP Symp.*, vol. 2, pp. 1162-1165, 1994.

[21] R. S. Adve, T. K. Sarkar, S. M. Rao, E. K. Miller and D. R. Pflug, "Application of the Cauchy method for extrapolating/interpolating narrow-band system responses," *IEEE Trans. Microwave Theory Tech.*, vol. 45, no. 5, pp. 837-845, May 1997.

[22] G. J. Burke, E. K. Miller and S. Chakrabarti, "Using model-based parameter estimation to increase the efficiency of computing electromagnetic transfer functions," *IEEE Trans. Mag.*, vol. 25, no. 4, pp. 2807-2809, Jul. 1989.

[23] T. Dhaene, J. Ureel, N. Faché and D. de Zutter, "Adaptive frequency sampling algorithm for fast and accurate S-parameter modeling of general planar structures," *IEEE Int. Microwave Symp. Dig.*, Orlando, FL, pp. 1427-1430, May 1995.

[24] E. K. Miller, "Model-based parameter estimation in electromagnetics: I—Background and theoretical development," *Applied Computational Electromagnetics Society Newsletter*, vol. 10, no. 3, pp. 40-63, Nov. 1995.

[25] E. K. Miller, "Minimizing the number of frequency samples needed to represent a transfer function using adaptive sampling," *12th Annual Review of Progress in Applied Computational Electromagnetics*, Naval Postgraduate School, Monterey, CA, pp. 1132-1139, 1996.

[26] J. de Geest, T. Dhaene. N. Faché and D. de Zutter, "Adaptive CAD-model building algorithm for general planar microwave structures," *IEEE Trans. Microwave Theory Tech.*, vol. 47, no. 9, pp. 1801-1809, Sep. 1999.

[27] D. H. Werner and R. J. Allard, "The simultaneous interpolation of antenna radiation patterns in both the spatial and frequency domains using model-based parameter estimation," *IEEE Trans. Antennas Propagat.*, vol. 48, no. 3, pp. 383-392, Mar. 2000.

[28] K. Kottapalli, T. K. Sarkar, Y. Hua, E. K. Miller and G. J. Burke, "Accurate computation of wide-band response of electromagnetic systems utilizing narrow-band information," *IEEE Trans. Microwave Theory Tech.*, vol. 39, no. 4, pp. 682-687, Apr. 1991.

[29] R. S. Adve and T. K. Sarkar, "Generation of accurate broadband information from narrowband data using the Cauchy method," *Microwave Opt. Technol. Lett.*, vol. 6, no. 10, pp. 569-573, 1993.

[30] U. Beyer and F. Śmieja, "Data exploration with reflective adaptive models," *Computational statistics data analysis*, vol. 22, pp. 193-211, 1999.

[31] R. Lehmensiek and P. Meyer, "An efficient adaptive frequency sampling algorithm for model-based parameter estimation as applied to aggressive space mapping," *Microwave Opt. Technol. Lett.*, vol. 24, no. 1, pp. 71-78, Jan. 2000.

[32] R. Lehmensiek and P. Meyer, "Using efficient model-based parameter estimation for pole-free solutions of modal propagation constants, as applied to shielded planar structures," *Appl. Comput. Electromagn. Soc. J. (ACES)*, accepted for publication, Mar. 2001.

[33] R. Lehmensiek and P. Meyer, "An efficient adaptive sampling algorithm for model-based parameter estimation as applied to computational electromagnetics," *First international workshop on surrogate modeling and space mapping for engineering optimization*, Lyngby, Denmark, Nov. 2000.

[34] R. Lehmensiek and P. Meyer, "Using efficient multivariate adaptive sampling by minimizing the number of CEM analyses needed to establish accurate interpolation models of microwave circuits," *IEEE Int. Microwave Symp. Dig.*, Phoenix, AZ, May 2001.

[35] R. Lehmensiek and P. Meyer, "Creating accurate multivariate rational interpolation models of microwave circuits by using efficient adaptive sampling to minimize the number of computational electromagnetic analyses," *IEEE Trans. Microwave Theory Tech.*, accepted for publication.

[36] W. Siemaszko, "Thiele-type branched continued fractions for two-variable functions," *J. Comp. Appl. Math.*, vol. 9, pp. 137-153, 1983.

[37] H. R. Schwarz, *Numerische Mathematik*, Stuttgart: B. G. Teubner, 1986.

[38] T. J. Rivlin, An introduction to the approximation of functions, New York: Dover, 1969.

[39] G. Blanch, "Numerical evaluation of continued fractions", *SIAM Rev.*, vol. 6, no. 4, pp. 383-421, Oct. 1964.

[40] A. Cuyt and B. Verdonk, "Multivariate reciprocal differences for branched Thiele continued fraction expansions," *J. Comp. Appl. Math.*, vol. 21, pp. 145-160, 1988.

[41] A. A. M. Cuyt and B. M. Verdonk, "A review of branched continued fraction theory for the construction of multivariate rational approximants," *Appl. Numer. Math.*, vol. 4, pp. 263-271, 1988.

[42] K. I. Kuchminskaya and W. Siemaszko, "Rational approximation and interpolation of functions by branched continued fractions," *Rational approximation and its applications in mathematics and physics*, J. Gilewicz, M. Pindor, W. Siemaszko, Eds., Lecture notes Math., 1237, pp.24-40, Berlin: Springer-Verlag, 1985.

[43] A. Ralston, "Rational Chebyshev approximation," *Mathematical methods for digital computers*, A. Ralston and H. S. Wilf (eds.), vol. 2, New York: John Wiley & Sons, 1960.

[44] J. W. Bandler, R. M. Biernacki, S. H. Chen, P. A. Grobelny and R. H. Hemmers, "Space mapping technique for electromagnetic optimization," *IEEE Trans. Microwave Theory Tech.*, vol. 42, pp. 2536-2544, 1994.

[45] J. W. Bandler, R. M. Biernacki, S. H. Chen, R. H. Hemmers and K. Madsen, "Electromagnetic optimization exploiting aggressive space mapping," *IEEE Trans. Microwave Theory Tech.*, vol. 43, no. 12, pp. 2874-2882, Dec. 1995.

[46] J. W. Bandler, R. M. Biernacki, S. H. Chen and Y. F. Huang, "Design optimization of interdigital filters using aggressive space mapping and decomposition," *IEEE Trans. Microwave Theory Tech.*, vol. 45, no. 5, pp. 761-769, May 1997.

[47] T. Itoh (ed.), Numerical techniques for microwave and millimeter-wave passive structures, New York: John Wiley & Sons, 1989.

[48] P. E. Gill, W. Murray and M. H. Wright, *Practical Optimization*, London: Academic Press, 1981.

[49] D. G. Corr and J. B. Davies, "Computer analysis of the fundamental and higher order modes in single and coupled microstrip," *IEEE Trans. Microwave Theory Tech.*, vol. 20, pp. 669-678, Oct. 1972.

[50] G. Essayag and B. Sauve, "Study of higher-order modes in a microstrip structure," *Electron. Lett.*, vol. 8, no. 23, pp. 564-566, Nov. 1972.

[51] C. J. Railton and T. Rozzi, "Complex modes in boxed microstrip," *IEEE Trans. Microwave Theory Tech.*, vol. 36, pp. 865-874, May 1988.

[52] E. Anemogiannis, E. N. Glytsis and T. K. Gaylord, "Efficient solution of Eigenvalue equations of optical waveguiding structures," *J. Lightwave Technol.*, vol. 12, no. 12, pp. 2080-2084, Dec. 1994.

[53] W-X. Huang and T. Itoh, "Complex modes in lossless shielded microstrip lines," *IEEE Trans. Microwave Theory Tech.*, vol. 36, no. 1, pp. 163-165, Jan. 1988.

[54] R. Sorrentino and M. Mongiardo, "Efficient and versatile analysis of microwave structures by combined mode matching and finite difference methods," *IEEE Microwave and Guided Wave Lett.,* vol. 3, no. 8, pp. 241-243, Aug. 1993.

[55] R. Beyer and F. Arndt, "The generalized scattering matrix separation technique combined with the MM/FE method for the efficient modal analysis of a comprehensive class of 3D passive waveguide circuits," *IEEE Int. Microwave Symp. Dig.*, Orlando, pp. 277-280, Jun. 1995.

[56] P. Meyer, "Solving microstrip discontinuities with a combined mode-matching and Method-of-Lines procedure," *Microwave Opt. Technol. Lett.*, vol. 8, no. 1, pp. 4-8, Jan. 1995.

[57] U. Rogge and R. Pregla, "Method of Lines for the analysis of dielectric waveguides," *J. Lightwave Technol.*, vol. 11, no. 12, pp. 2015-2020, Dec. 1993.

[58] R. Pregla and W. Pascher, *Numerical techniques for microwave and millimetre-wave passive structures*, (editor T Itoh), New York: John Wiley and Sons, pp.380-446, 1989.

[59] P. Meyer, "A combined mode-matching and Method-of-Lines procedure for the analysis of planar microwave circuits", Ph. D. Dissertation, University of Stellenbosch, 1995.

[60] W. J. A. van Brakel, "Solving three-layer planar microwave structures with the Method-of-Lines", Master Thesis, University of Stellenbosch, 1998.

[61] C. A. Olley and T. E. Rozzi, "Systematic characterisation of the spectrum of unilateral finline," *IEEE Trans. Microwave Theory Tech.*, vol. 34, pp. 1147-1156, Nov. 1986.

[62] V. A. Labay and J. Bornemann, "Matrix singular value decomposition for pole-free solutions of homogenous matrix equations as applied to numerical modelling methods," *IEEE Microwave and Guided Wave Lett.*, vol. 2, no. 2, pp. 49-51, Feb. 1992.

[63] R. Fletcher, *Practical methods of optimization*, Chichester: John Wiley & Sons, 1987.

[64] G. Peters and J. H. Wilkinson, "Practical problems arising in the solution of polynomial equations," *J. Inst. Math. Appl.*, vol. 8, pp. 16-35, 1971.

[65] F. Oberhettinger and W. Magnus, *Anwendung der Elliptischen Funktionen in Physik und Technik*, Berlin: Springer-Verlag, 1949.

[66] B. Bhat and S. K. Koul, *Analysis, design, and applications of fin lines*, Norwood: Artech House Inc., 1987.

[67] Y. Leviatan, P. G. Li, A. T. Adams and J. Perini, "Single-post inductive obstacle in rectangular waveguide," *IEEE Trans. Microwave Theory Tech.*, vol. 31, no. 10, pp. 806-811, Oct. 1983.

[68] W. L. Stutzman and G. A. Thiele, *Antenna theory and design*, 2nd ed., New York: John Wiley & Sons, 1998.

[69] J. W. Bandler and S. H. Chen, "Circuit optimization: the state of the art," (invited), *IEEE Trans. Microwave Theory Tech.*, vol. 36, no. 2, pp. 424-443, Feb. 1988.

[70] M. H. Bakr, J. W. Bandler, K. Madsen and J. Søndergaard, "Review of the space mapping approach to engineering optimization and modeling," *Optimization and Engineering*, vol. 1.3, 2000.

[71] C. G. Broyden, "A class of methods for solving nonlinear simultaneous equations," *Math. Comput.*, vol. 19, no. 92, pp. 577-593, Oct. 1965.

APPENDIX A: SPACE MAPPING OPTIMISATION

A.1 Introduction

Different models, a "coarse" model and a "fine" model, may often describe a microwave circuit. The fine model is considered very accurate but computationally very intensive, while the coarse model is simple and fast but less accurate or has limited validity range. The coarse model may be an empirical circuit-theoretic model or a coarse-resolution CEM model. The fine model typically is a CEM field-theoretic model, or it can be a lab measurement. Coarse models are suitable for iterative design optimisation, while fine models are often limited to design validation due to their high computational cost.

Space mapping provides a link between the coarse and the fine models. The technique combines the accuracy of the fine model with the speed of the coarse model. The bulk of CPU intensive optimisation is done in the coarse model parameter space.

A.2 Space Mapping Theory [44]

Let the coarse model and fine model input parameters be denoted by vectors $\mathbf{x}_{os}$ and $\mathbf{x}_{em}$ respectively. $\mathbf{x}_{os}$ is defined in the optimisation space $\mathbf{X}_{os}$. $\mathbf{x}_{em}$ is defined in the CEM space $\mathbf{X}_{em}$. The $\mathbf{X}_{os}$ space and the $\mathbf{X}_{em}$ space model response vectors are denoted by $\mathbf{R}_{os}(\mathbf{x}_{os})$ and $\mathbf{R}_{em}(\mathbf{x}_{em})$ respectively. $\mathbf{R}_{em}(\mathbf{x}_{em})$ is considered very accurate but computationally very intensive while $\mathbf{R}_{os}(\mathbf{x}_{os})$ is fast but less accurate.

Space mapping (SM) needs to find a mathematical link between the input parameters of the coarse model and the input parameters of the fine model. Define a non-linear vector function P that maps the input parameters of the fine model onto the input parameters of the coarse model as follows:

$$\mathbf{x}_{os} = P(\mathbf{x}_{em}) . \tag{22}$$

The Space mapping problem is then, to find the mapping so that the responses of the two models are the same, i.e.

$$\mathbf{R}_{os}(P(\mathbf{x}_{em})) \approx \mathbf{R}_{em}(\mathbf{x}_{em}) . \tag{23}$$

The input parameter $\mathbf{x}_{os}^{*}$, which produces the optimal response in $\mathbf{X}_{os}$, is determined by performing conventional design optimisation entirely in the $\mathbf{X}_{os}$ space [69]. The inverse mapping P^{-1} is used to find the SM solution in $\mathbf{X}_{em}$ from $\mathbf{x}_{os}^{*}$, as shown in equation (24). The mapped solution $\bar{\mathbf{x}}_{em}$ may

not be the true optimum $\mathbf{x}_{em}^{*}$.

$$\bar{\mathbf{x}}_{em} = \mathrm{P}^{-1}(\mathbf{x}_{os}^{*}) \approx \mathbf{x}_{em}^{*}. \tag{24}$$

The analytical form of P is not available and has to be found by an iterative process, starting from the point $\mathbf{x}_{em}^{(1)} = \mathbf{x}_{os}^{*}$. At the j^{th} iteration, $\mathbf{x}_{em}^{(j)}$ is obtained by applying P^{-1} using the current estimate of P, namely $\mathrm{P}^{(j)^{-1}}$,

$$\mathbf{x}_{em}^{(j)} = \mathrm{P}^{(j)^{-1}}(\mathbf{x}_{os}^{*}). \tag{25}$$

The SM solution is reached when the CEM analysis at $\mathbf{x}_{em}^{(j)}$ produces the desired response, i.e.

$$\left\| \mathbf{R}_{os}(\mathbf{x}_{os}^{*}) - \mathbf{R}_{em}(\mathbf{x}_{em}^{(j)}) \right\| \leq \varepsilon, \tag{26}$$

where $\|\cdot\|$ indicates a suitable norm and ε is a small positive constant. The two models are now aligned and equation (24) is used to determine the input parameter in $\mathbf{X}_{em}$,

$$\bar{\mathbf{x}}_{em} = \mathbf{x}_{em}^{(j)}, \tag{27}$$

With no solution reached, parameter extraction is used to determine $\mathbf{x}_{os}^{(j)}$ as follows:

$$\min_{\mathbf{x}_{os}^{(j)}} \left\| \mathbf{R}_{os}(\mathbf{x}_{os}^{(j)}) - \mathbf{R}_{em}(\mathbf{x}_{em}^{(j)}) \right\|, \tag{28}$$

In words, parameter extraction determines the input parameters of the coarse model, $\mathbf{x}_{os}^{(j)}$, whose response matches the fine model response at $\mathbf{x}_{em}^{(j)}$. $\mathbf{x}_{os}^{(j)}$ is determined through optimisation in $\mathbf{X}_{os}$ from the data provided by the CEM analysis at $\mathbf{x}_{em}^{(j)}$.

Having determined $\mathbf{x}_{em}^{(j)}$ and $\mathbf{x}_{os}^{(j)}$, the mapping P at the j^{th} iteration is calculated. Various methods have been proposed to determine P [70]. In this dissertation the aggressive space mapping technique (ASM) is used and is discussed in section A.3. The ASM optimisation process is illustrated graphically in Fig. A1.

A.3 Aggressive Space Mapping [45]

The aggressive space mapping algorithm aggressively uses every CEM analysis to optimise the design. A quasi-Newton iteration in conjunction with first-order derivative approximations updated by the classic Broyden formula refines the mapping.

Define a set of non-linear equations:

$$\mathrm{f}(\mathbf{x}_{\mathrm{em}}) = \mathrm{P}(\mathbf{x}_{\mathrm{em}}) - \mathbf{x}_{\mathrm{os}}^{*}. \tag{29}$$

As the SM algorithm converges to a SM solution, $\mathbf{x}_{\mathrm{os}}^{(j)} \rightarrow \mathbf{x}_{\mathrm{os}}^{*}$. The goal is $\mathbf{x}_{\mathrm{os}}^{(j+1)} = \mathbf{x}_{\mathrm{os}}^{*}$ or

$$\mathrm{f}\left(\mathbf{x}_{\mathrm{em}}^{(j+1)}\right) = 0. \tag{30}$$

A quasi-Newton iteration is used to solve the set of non-linear equations in (30). Assuming f can be linearised locally, the next iterate is:

$$\mathbf{x}_{\mathrm{em}}^{(j+1)} = \mathbf{x}_{\mathrm{em}}^{(j)} + \mathbf{h}^{(j)}, \tag{31}$$

where $\mathbf{h}^{(j)}$ solves the linear system

$$\mathbf{B}^{(j)}\mathbf{h}^{(j)} = -\mathrm{f}\left(\mathbf{x}_{\mathrm{em}}^{(j)}\right). \tag{32}$$

This follows from the Taylor series expansion of (28) about $\mathbf{x}_{\mathrm{em}}^{(j)}$ (ignoring higher order derivatives): $\mathrm{f}\left(\mathbf{x}_{\mathrm{em}}^{(j)} + \mathbf{h}^{(j)}\right) \approx \mathrm{f}\left(\mathbf{x}_{\mathrm{em}}^{(j)}\right) + \mathrm{J}\left(\mathbf{x}_{\mathrm{em}}^{(j)}\right)\mathbf{h}^{(j)}$. $\mathbf{B}^{(j)}$ approximates the Jacobian matrix

$$\mathrm{J}(\mathbf{x}_{\mathrm{em}}^{(j)}) = \left[\frac{\partial \mathrm{f}^{T}(\mathbf{x}_{\mathrm{em}})}{\partial \mathbf{x}_{\mathrm{em}}}\right]^{T}\Bigg|_{\mathbf{x}_{\mathrm{em}}=\mathbf{x}_{\mathrm{em}}^{(j)}}. \tag{33}$$

Adapting the Broyden formula [71], $\mathbf{B}$ is updated according to equation (34) and initialised with $\mathbf{B}^{(0)}$ equal to the identity matrix.

$$\mathbf{B}^{(j+1)} = \mathbf{B}^{(j)} + \frac{\mathrm{f}\left(\mathbf{x}_{\mathrm{em}}^{(j+1)}\right)\mathbf{h}^{(j)T}}{\mathbf{h}^{(j)T}\mathbf{h}^{(j)}} \tag{34}$$

A.4 ASM assumptions

- A coarse model and a fine model are available
- $\mathbf{X}_{\mathrm{os}}$ and $\mathbf{X}_{\mathrm{em}}$ have the same dimensionality
- $\mathbf{x}_{\mathrm{os}}$ and $\mathbf{x}_{\mathrm{em}}$ describe the same physical parameters
- P exists and is one-to-one within some local modelling region encompassing the SM solution
- for a given $\mathbf{x}_{\mathrm{em}}$ its image $\mathbf{x}_{\mathrm{os}}$ can be found by a suitable parameter extraction procedure and this process is unique

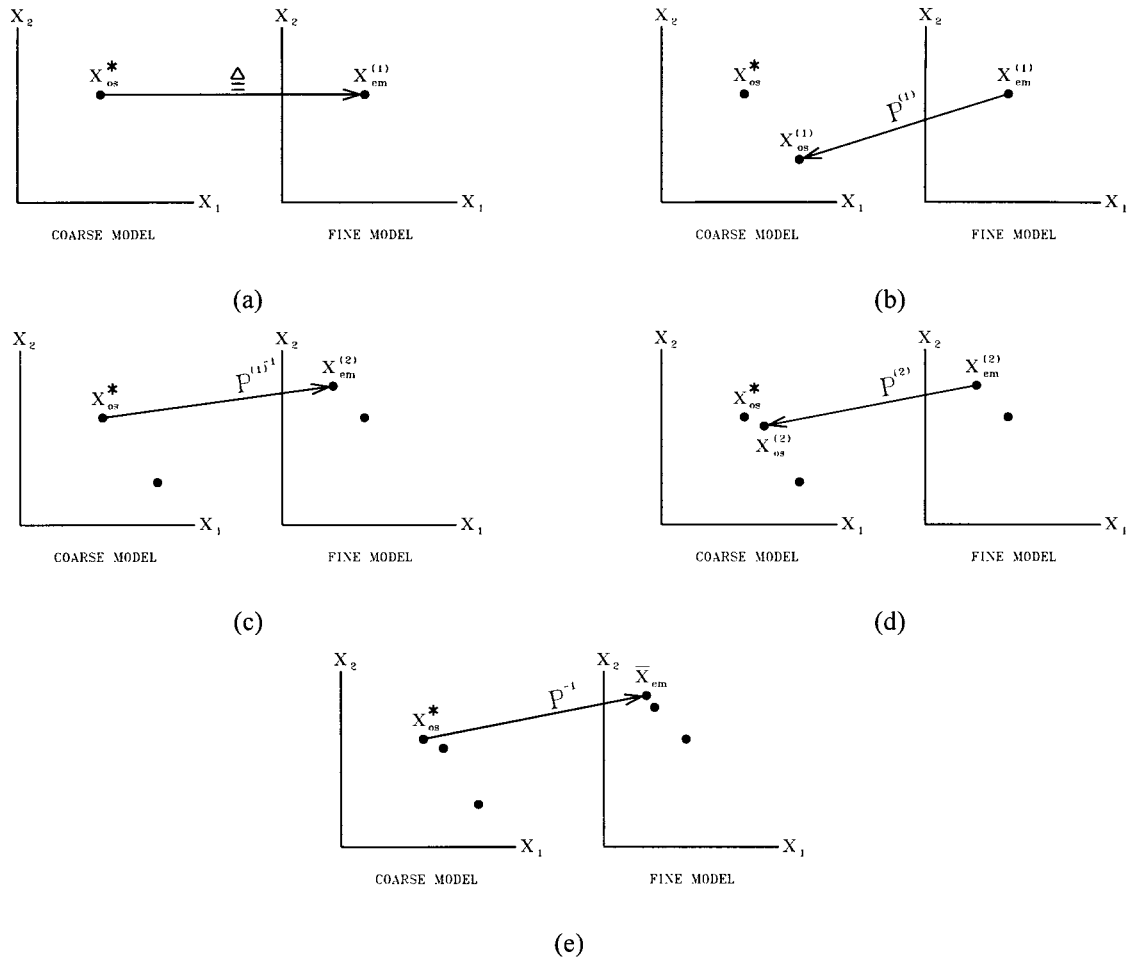

Fig. A1. Illustration of aggressive space mapping: (a) initialisation, (b) performing coarse model parameter extraction to match the fine model response, (c) applying the inverse transformation to obtain the fine model point, (d) performing coarse model parameter extraction, (e) applying the updated inverse transformation.

A.5 Implementation of the ASM algorithm

Initialise: $\mathbf{x}_{em}^{(1)} = \mathbf{x}_{os}^{*}$

$\mathbf{B}^{(1)} = \mathbf{I}$ (the identity matrix)

$\mathrm{f}\left(\mathbf{x}_{em}^{(1)}\right) = \mathrm{P}\left(\mathbf{x}_{em}^{(1)}\right) - \mathbf{x}_{os}^{*}$

$j = 1$

Stop if $\left\|\mathrm{f}\left(\mathbf{x}_{em}^{(1)}\right)\right\| \le \eta$

Iteration j: Solve $\mathbf{B}^{(j)}\mathbf{h}^{(j)} = -\mathrm{f}\left(\mathbf{x}_{em}^{(j)}\right)$ for $\mathbf{h}^{(j)}$

Set $\mathbf{x}_{em}^{(j+1)} = \mathbf{x}_{em}^{(j)} + \mathbf{h}^{(j)}$

Compute $\mathrm{f}\left(\mathbf{x}_{em}^{(j+1)}\right) = \mathrm{P}\left(\mathbf{x}_{em}^{(j+1)}\right) - \mathbf{x}_{os}^{*}$

Stop if $\left\|\mathrm{f}\left(\mathbf{x}_{em}^{(j+1)}\right)\right\| \le \eta$

Update $\mathbf{B}^{(j)}$ to $\mathbf{B}^{(j+1)}$

Set $j = j + 1$; Next iteration.

η is a small positive constant.